

# POLITECNICO DI MILANO

Scuola di Ingegneria Industriale e Dell'Informazione

Master Thesis in Materials Engineering and Nanotechnology

Dipartimento Di Chimica, Materiali e Ingegneria Chimica "Giulio Natta"



## SHORT TERM ANALYTICAL METHODS FOR POLYMER THERMAL ENDURANCE PREDICTION IN DIFFERENT ENVIRONMENTS

**Supervisor:** Prof. Francesco Briatico Vangosa

**Co-supervisor:** Ing. Stefano Tagliabue

Tobia Mariotto

ID 875606

Academic Year 2018/2019

# Table of contents

<b>CHAPTER 1-</b>	<b>Introduction and state of art.....</b>	<b>9</b>
1.1	Polymer degradation.....	9
1.1.1	Thermal degradation.....	9
1.1.2	Oxidation.....	10
1.1.3	Mechanical degradation.....	12
1.1.4	Photodegradation.....	13
1.2	Thermal analysis.....	14
1.2.1	Thermogravimetry (TG) .....	15
1.2.1.1	Procedure.....	15
1.2.1.2	Kinetic Parameters.....	18
1.2.2	Long-term analysis.....	25
1.2.3	Differential thermal analysis (DTA) .....	26
1.2.4	Differential scanning calorimetry (DSC) .....	28
1.3	Purpose of the work.....	30
<b>CHAPTER 2-</b>	<b>Materials and methods.....</b>	<b>32</b>
2.1	Materials.....	32
2.1.1	High-density polyethylene.....	32
2.1.2	Polystyrene N2982 and N2380.....	33
2.2	Thermogravimetric analysis.....	36
2.3	Molecular weight estimation.....	40
2.3.1	Melt flow index .....	40
2.3.2	Determination of intrinsic viscosity.....	41
2.4	Thermo-mechanical degradation.....	44
2.5	Applicability of Ozawa-Flynn-Wall method.....	46

<b>CHAPTER 3- Experimental results.....</b>	<b>48</b>
3.1 Thermo-gravimetric analysis.....	48
3.1.1 High-density polyethylene.....	48
3.1.2 Polystyrene N2982.....	49
3.1.3 Polystyrene N2380.....	50
3.2 Melt flow index.....	52
3.3 Viscometer.....	55
<b>CHAPTER 4- Analysis and discussion.....</b>	<b>58</b>
4.1. Thermogravimetric Analysis.....	58
4.1.1 Polystyrene N2982.....	58
4.1.2 Polystyrene N2380.....	61
4.1.3 High-density polyethylene.....	63
4.2. Applicability of Ozawa-Flynn-Wall method.....	65
4.2.1. Polystyrene N2982.....	66
4.2.2. Polystyrene N2380.....	67
<b>CHAPTER 5- Conclusions.....</b>	<b>69</b>
<b>REFERENCES.....</b>	<b>71</b>

## Table of figures

<b>Figure 1.</b>	Branching reaction of polypropylene [15].....	11
<b>Figure 2.</b>	Termination reaction of polyethylene [16].....	11
<b>Figure 3.</b>	Typical example of photodegradation reaction.....	13
<b>Figure 4.</b>	Example of thermogravimetric curve [27] .....	15
<b>Figure 5.</b>	Example of differential thermogravimetric curve [27].....	15
<b>Figure 6.</b>	Example of polycarbonate thermograms obtained for low (black) and high heating rate.....	16
<b>Figure 7.</b>	Example of PMMA thermograms obtained for samples with different mass [97]...17	
<b>Figure 8.</b>	Example of thermograms obtained in air and N <sub>2</sub> atmosphere for polycarbonate....18	
<b>Figure 9.</b>	Example of DTG obtained in air and N <sub>2</sub> atmosphere for polycarbonate .....	18
<b>Figure 10.</b>	Representative plot of impact, tensile and dielectric strength decay over time for a specimen subjected to constant temperature field [75].....	25
<b>Figure 11.</b>	Example of differential thermal analysis plot.....	27
<b>Figure 12.</b>	Schematic representation of DTA apparatus.....	27
<b>Figure 13.</b>	Example of differential scanning calorimetry thermogram [55] .....	28
<b>Figure 14.</b>	Schematic representation of differential scanning calorimetry apparatus.....	29
<b>Figure 15.</b>	Molecular structure of polyethylene.....	32
<b>Figure 16.</b>	Molecular structure of polystyrene.....	33
<b>Figure 17.</b>	$\beta$ -scission reactions.....	34
<b>Figure 18.</b>	Intermolecular (above) and intramolecular (below) hydrogen abstraction reactions [58].....	35
<b>Figure 19.</b>	Example of thermogravimetric curves for different heating rates. The lowest one is one the left.....	36
<b>Figure 20.</b>	Example of experimental plot obtained using Equation 11.....	37
<b>Figure 21.</b>	Example of thermal endurance curve.....	39
<b>Figure 22.</b>	Representation of main component of melt flow indexer.....	41
<b>Figure 23.</b>	Schematic representation of capillary viscometer apparatus.....	42
<b>Figure 24.</b>	Representation of a BS/IP/MSL viscometer [73].....	42
<b>Figure 25.</b>	Example of plot used to estimate intrinsic viscosity [71] .....	43

<b>Figure 26.</b> Schematic representation of Brabender mixer chamber: above (left) and front view (right) [84] .....	44
<b>Figure 27.</b> Typical torque rheometer fusion test curve [84] .....	45
<b>Figure 28.</b> Standard TGA (left) and DTG (right) of HDPE performed at 1°C/min, 2°C/min, 3°C/min, 5°C/min, 7°C/min, 10°C/min in nitrogen atmosphere.....	48
<b>Figure 29.</b> Standard TGA (continuous line) and DTG (dotted line) of HDPE [93].....	48
<b>Figure 30.</b> Standard TGA (left) and DTG (right) of polystyrene N2982 performed at 1°C/min, 2°C/min, 3°C/min, 5°C/min, 7°C/min, 10°C/min, 15°C/min and 20°C/min in nitrogen atmosphere.....	49
<b>Figure 31.</b> Standard TGA (right) and DTG (left) of polystyrene N2982 performed at 1°C/min, 2°C/min, 3°C/min, 5°C/min, 7°C/min, 10°C/min in oxygen atmosphere.....	49
<b>Figure 32.</b> Standard TGA (left) and DTG (right) of polystyrene N2380 performed at 1°C/min, 2°C/min, 3°C/min, 5°C/min, 7°C/min, 10°C/min, 15°C/min and 20°C/min in nitrogen atmosphere.....	50
<b>Figure 33.</b> Standard TGA (right) and DTG (left) of polystyrene N2380 performed at 1°C/min, 2°C/min, 3°C/min, 5°C/min, 7°C/min, 10°C/min in oxygen atmosphere.....	50
<b>Figure 34.</b> Comparison of TGA of PS N2982 (black) and PS N2380 (red) at 1°C/min and 10°C/min performed in nitrogen (left) and air (right).....	51
<b>Figure 35.</b> Cut thread masses resulting from MFI test (200°C, 5kg) for PS N2982 (left) and PS N2380 (right).....	52
<b>Figure 36.</b> Cut thread masses resulting from MFI test (180°C/ 5kg) for PS N2982 (left) and PS N2380 (right).....	52
<b>Figure 37.</b> Cut thread masses resulting from MFI test (180°C/ 5kg) for PS N2982.....	53
<b>Figure 38.</b> Cut thread masses resulting from MFI test (190°C/ 21.6 kg) for HDPE.....	53
<b>Figure 39.</b> Experimental plot to determine intrinsic viscosity of PS N2982 (left) and PS N2380 (right).....	55
<b>Figure 40.</b> Experimental plot to determine intrinsic viscosity of PS N2982 after being subjected to mechanical stress.....	56
<b>Figure 41.</b> Plot of heating rate as function of temperature reciprocal in nitrogen (left) and air (right) for $\alpha$ = 2%, 5%, 10%, 30%, 40%, 50% and 75%, ordered from right to left.....	58
<b>Figure 42.</b> Plot of activation energies obtained with OFW method as function of mass loss percentage in nitrogen (black) and air (red).....	59
<b>Figure 43.</b> Thermal endurance curves of PS 2982 in nitrogen (left) and air environment (right) for conversion percentages of 2%, 5%, 10%, 30%, 40%, 50% and 75%, ordered from left to right.....	60

<b>Figure 44.</b> Plot of heating rate as function of reciprocal of temperatures obtained for heating rate range of 1-20°C/min.....	60
<b>Figure 45.</b> Plot of activation energies obtained for heating rate range of 1-10°C/min (red) and 1-20°C/min (black).....	60
<b>Figure 46.</b> TE curves for conversion rates of 10% and 50% of PS 2982 obtained with activation energy obtained by employing TGA curves in range of 1-10°C/min (black) and 1-20°C/min (red).....	61
<b>Figure 47.</b> Plot of activation energies of PS N2982 (black) and PS N 2380 (red) in nitrogen (left) and air environment (right).....	62
<b>Figure 48.</b> Thermal endurance curves of PS 2982 in nitrogen (left) and air environment (right) for conversion percentages of 10% and 50%.....	63
<b>Figure 49.</b> Plot of activation energies for HDPE degradation in N <sub>2</sub> as function of mass loss percentage.....	63
<b>Figure 50.</b> Thermal endurance curves of HDPE in nitrogen (left) and air environment (right) for conversion percentages of 2%, 5%, 10%, 30%, 40%, 50% and 75%, ordered from left to right.....	64
<b>Figure 51.</b> Degradation percentages of samples S1 (red), S2 (blue), S3 (violet) and S4 (green) for PS N2982 compared to the ones obtained by mean of OFW (black) obtained for PS N2982 (left) and PS N2380 (right).....	65
<b>Figure 52.</b> Degradation percentages of sample S1 obtained experimentally (black) and by mean of the proposed method.....	66
<b>Figure 53.</b> Degradation percentages of sample S2 obtained experimentally (black) and by mean of the proposed method.....	66
<b>Figure 54.</b> Degradation percentages of sample S3 obtained experimentally (black) and by mean of the proposed method.....	66
<b>Figure 55.</b> Degradation percentages of sample S4 obtained experimentally (black) and by mean of the proposed method.....	66
<b>Figure 56.</b> Relation between shift factor and area-volume ratio for PS N2982.....	67
<b>Figure 57.</b> Degradation percentages of sample S1 obtained experimentally (black) and by mean of the proposed method.....	67
<b>Figure 58.</b> Degradation percentages of sample S2 obtained experimentally (black) and by mean of the proposed method.....	67
<b>Figure 59.</b> Degradation percentages of sample S3 obtained experimentally (black) and by mean of the proposed method.....	68

**Figure 60.** Degradation percentages of sample S4 obtained experimentally (black) and by mean of the proposed method.....68

**Figure 61.** Relation between shift factor and area-volume ratio for PS N2380.....68

## Abstract

Polymers are a class of materials that can find countless applications in various fields due to their low cost, versatility and ease of processing, although, their properties are strongly dependent on both their processing and service environment.

During processing (e.g. extrusion) a polymer is subjected to a complex set of environmental conditions, which include high temperature fields, oxidative environment and mechanical shear stress, features that could lead to degradation of the material.

During service life, harsh environment like high temperatures and solar irradiation in air atmosphere cause material degradation.

This behavior is generally coupled with a mass loss related to the release of decomposition products.

Mass variation in different environments can be studied by means of thermogravimetric analysis: a rather recent technique that allows to evaluate in a short time the thermal stability of a substance subjected to different temperatures and environments.

The most important result obtainable by an appropriate elaboration of TGA outcome is the thermal endurance, which provides an estimation of the service life of a substance subjected to a constant temperature in a certain atmosphere.

In this work the thermal stability of polystyrene (PS) will be studied in inert and oxidative environment, furthermore, an initial evaluation of the effect of applied stress will be provided.

## Sommario

I polimeri sono una classe di materiali che trova diverse applicazioni in vari campi grazie alla loro versatilità, semplicità di lavorazione e basso costo, sebbene le loro proprietà siano fortemente dipendenti sia dai metodi di lavorazione che dall'ambiente d'utilizzo.

Durante il processo di lavorazione (e.g. estrusione) il materiale polimerico è soggetto ad una complessa serie di condizioni ambientali, che includono alte temperature, ambienti ossidativi e sforzi di taglio meccanici, caratteristiche che possono portare alla prematura degradazione del materiale. Questo comportamento è generalmente associato a una perdita di massa correlata al rilascio dei prodotti di degradazione.

La variazione della massa in diversi ambienti può essere studiata per mezzo di un'analisi termogravimetrica (TGA): una tecnica piuttosto recente che permette di valutare in breve tempo la stabilità termica, in termini di perdita di massa, di una sostanza sottoposta a diverse temperature e condizioni ambientali.

Il risultato principale ottenibile da un'appropriata elaborazione dei risultati della TGA è la cosiddetta "thermal endurance", che fornisce una stima della vita di servizio di una sostanza soggetta a condizioni termiche e ambientali costanti.

In questo progetto verrà studiata la stabilità termica del polistirene (PS) in ambiente inerte e ossidativo, inoltre, verrà fornita una valutazione iniziale dell'effetto dell'applicazione di uno sforzo di taglio.

# 1. Introduction and state of art

## 1.1. Polymer degradation

Degradation is defined as unrecoverable chemical transformation in molecular weight, chemical composition and structure to which a polymer can undergo due to external factors such as heat, air, mechanical loading, electromagnetic radiation, etc. In practice this might result in a change in its appearance (e.g. texture, color) and a loss in mechanical properties (e.g. tensile and flexural strength, impact resistance). When, instead, transformation is caused by physical factor, such as free-volume relaxation, a different process, called physical aging, takes place.

Environmental parameters (e.g. atmosphere, temperature) highly influence degradation reaction to which the material is subjected: aggressive condition can lead to rupture of the weakest bonds in the polymeric chain, consequently forming highly reactive species, called radicals.

Lots of other factors affect degradation rate during service life, such as chemical structure, presence of structural defects, impurities (e.g. polymerization catalyst residues) and the use of stabilizers. Several researches have shown that polymer degradative processes are always preceded by an induction time, characteristic of each substance, during which no degradative process occur.

In this work the focus will be given to three different degradation mechanisms and methods to forecast their magnitude: thermal, oxidative and thermo-mechanical degradation.

### 1.1.1. Thermal degradation

In this kind of degradation, the reaction driving force is provided by a temperature field characterized by a magnitude high enough to overcome bond energy, resulting in bond breaking and, hence, degradation in terms of mass loss. Generally, the changes associated with thermal degradation of polymers follow a series of chemical reactions via chain scission of the macromolecules. Chain-scission reactions usually follow a multistep free-radical route comprised of initiation, propagation, and termination steps [1].

- **Initiation:** it is characterized by free radical formation due to random rupture of weak sites within the chain backbone or at the chain end.

The first case is known as random scission and is characterized by formation of oligomers as degradation products; polyethylene (PE), polyethylene terephthalate (PET) and polystyrene are three examples of polymers showing this behavior.

Chain-end degradation, instead, (generally known as unzipping) can occur only in polymeric chains containing active chain-end (i.e. radical) and is characterized by formation of monomers as degradation products; polymethyl methacrylate

(PMMA) and polytetrafluoroethylene (PTFE) are two examples of polymers showing this behavior [2].

- **Propagation:** it is characterized by several possible simultaneous reactions between different chains (i.e. cross-linking, main-chain unsaturation, intramolecular or intermolecular hydrogen transfer) or within the same chain (i.e. further degradation of the main chain due to unzipping or random scission).  
In case of particular polymers (e.g. polyvinyl chloride), moreover, side-chain cyclization reactions may take place.  
Generally mechanical properties are only affected by main chain reactions, while side-chain ones only influence color.
- **Termination:** it is characterized by the removal of reactive radical species. It may occur by means of radical coupling (recombination) or disproportionation [1]

### 1.1.2. Oxidation

Polymer oxidation is defined as the degradation process that occurs in the presence of oxygen. This element acts as an accelerant for the degradation process, decreasing molecular weight and introducing carboxyl or hydroxyl groups in the polymeric chain [3,4,5].

The reaction mechanism has been studied by Bolland and Gee in 1946 [6,7] and, as for thermal degradation, follows a multistep free-radical route comprised of initiation, propagation, branching and termination steps.

- **Initiation:** in this stage oxygen is not involved; indeed, free radicals are generated by thermal stress or by the combined action of mechanical and thermal stress [8].



- **Propagation:** it is a repeating reaction characterized by two sub-reactions, which are described as:



Given that the peroxy radical formation reaction [2] is characterized by a very high reaction rate, the total propagation process is hindered by the hydroperoxide formation [3], that is determined by the probability of hydrogen abstraction. Carbon-hydrogen bond strength is the main feature affecting this last reaction: low strength bonds are more oxidizable as the forming radical has increased stability. Several studies have been performed on propagation reactions. For instance, Mayo [11] and Garton [12] found a relation with the chain mobility, showing that only a

portion (16% for Mayo and 4.5% for Garton) of the peroxy radicals (generally produced as pairs) can cause propagation reaction.

This effect is to attribute to the radical formation process: they are formed in pairs and can stay under each other's influence for a long time and give recombination reactions [9,10].

- **Branching:** it is characterized by the hydroperoxide decomposition reaction (4), which increases the oxidation rate by formation of new radicals.



This reaction can be described by several mechanisms according to the site where propagation reaction takes places [13,14].

For instance, in the oxidation of polypropylene (PP), the propagation reaction brings to the formation of adjacent hydroperoxides, which can decompose through a bi-functional reaction with a lower activation energy than unimolecular decomposition [15].

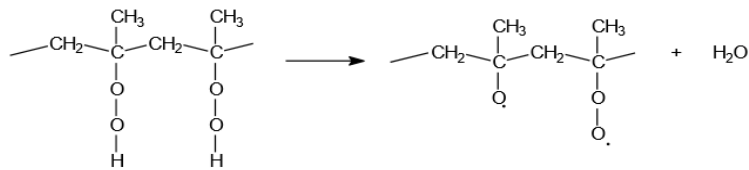


Figure 1. Branching reaction of polypropylene [15]

- **Termination:** it is a complex bimolecular reaction that, in presence of sufficient oxygen concentration, can be reduced to a simple reaction between two peroxy radicals [3].



This reaction can lead to different products. An example is given for PE [16], which terminates according to the Russel mechanism forming a ketone and an alcohol.

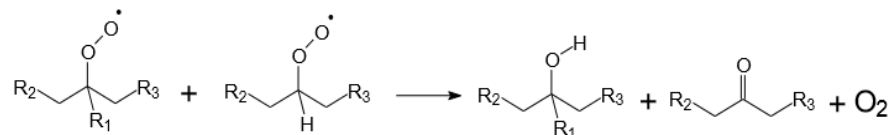


Figure 2. Termination reaction of polyethylene [16]

In case of limited oxygen amount, as for polymer processing conditions, other radicals than peroxy ones can cause termination.

### 1.1.3. Mechanical degradation

Mechanical degradation refers to any kind of decay occurring to a polymer due to applied mechanical action (mostly at high temperatures during processing). Because of velocity gradients generated during flow, polymeric chains become extended and can undergo to rupture, forming two radicals [17].



Although, according to Bird et al. [18], no reliable quantitative theory of mechanical stability of polymers exists, a qualitative description of this phenomenon can be provided.

Generally, chain tearing occurs in those sites characterized by weak bonds, such as [19]:

- Side chain linkages to main chain (i.e. branch point)
- Crosslink point
- Point of inclusion of heteroatoms or quaternary carbon atoms
- Dissymmetry between adjacent atoms

As was pointed out by Frenkel et al. [20], the chain breaking probability is directly proportional on the degree of polymerization (i.e. chain length): polymer molecular weight decreases less for lower molecular weight until reaching a limiting value under which mechanical degradation is not possible.

Mechanical degradation effect is strongly dependent on other degradation mechanisms:

- In inert environment (e.g. nitrogen) at low temperatures recombination reaction take place, hence concluding degradation propagation



- In reactive environment (e.g. oxygen) radical species react with oxygen, bringing to an acceleration of the degradation process



Degradation rate can be affected by several factor, such as applied shear stress, as shown from Capone et al [21]. According to their work the extruding rate (i.e. applied stress) is inversely proportional to the molecular mass reduction and, hence, to the degradation rate.

Another example has been provided by Arisawa et al. work [22,23], according which polymer molecular weight highly influences the degradation rate which increases for longer polymeric chain.

### 1.1.4. Photodegradation

Photodegradation refers to a class of reaction in which the driving force is provided by electromagnetic radiation (generally UV or more rarely visible light) and result in rupture of molecular bonds within a polymeric chain (e.g. molecular weight reduction, side group elimination). This process, as for mechanical degradation, is often coupled with other degradation mechanism (e.g. photo-oxidation) for which behaves as an activator.

Photodegradation is an homolytic reaction in which chain weaker bonds undergoes breakage and form two radical species.

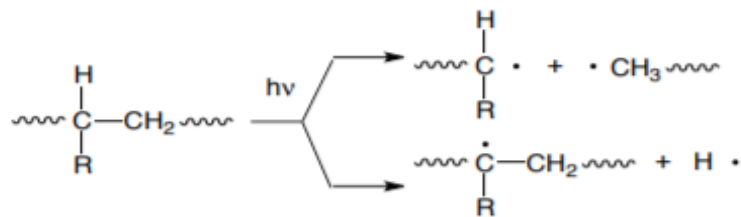


Figure 3. Typical example of photodegradation reaction

A very important role is also played by impurities contained in the polymeric matrix, which may hinder or even initiate degradation process. Generally, the addition of fillers and pigment, such as carbon black, result in an improvement of UV stability. On the other hand, substances that absorb UV radiation, such as ketones, quinones and peroxides, behave as initiators.

Photodegradation occurs mainly on the exposition surface with development of cracks and discoloration, leading to a quick loss of mechanical properties [24].

## 1.2 Thermal analysis

Thermal analysis is defined by the International Confederation of Thermal Analysis (ICTA) as “a set of techniques where a physical or chemical property is determined and controlled in function of time, temperature or heat flow” [25]. This class of tests was firstly introduced in the late 19<sup>th</sup> century by Le Chatelier, but the main development occurred in the beginning of '70s [26].

Nowadays, thermal analysis is an essential tool for material research and development, allowing to analyze a great number of properties, such as physical and chemical stability, change of phase and fundamental kinetic parameters.

Different procedure exists to examine the effect of the addition of heat to the system physical properties. For this reason, ICTA provided a classification, reported in Table 1, based on the studied property (e.g. mass, temperature, enthalpy, mechanical characteristics).

Physical property	Derived technique (s)	Accepted abbreviation
Mass	Thermogravimetry	TG
	Isobaric mass-change determination	
	Evolved gas detection	EGD
	Evolved gas analysis	EGA
	Emanation thermal analysis	
Temperature	Thermoparticulate analysis	
	Heating-curve determination	
	Differential thermal analysis	DTA
Enthalpy	Differential scanning calorimetry	DSC
Dimensions	Thermodilatometry	
Mechanical characteristics	Thermomechanical analysis	TMA
	Dynamic thermoméchanometry	
Acoustic characteristics	Thermosonimetry	
	Thermoacoustimetry	
Optical characteristics	Thermoptometry	
Electrical characteristics	Thermoelectrometry	
Magnetic characteristics	Thermomagnetometry	

Table 1. Different thermal analysis techniques classified according to evaluated physical properties [50]

Among these techniques, the most widely used are by far thermogravimetry, differential scanning calorimetry and differential thermal analysis.

## 1.2.1 Thermogravimetry

### 1.2.1.1 Procedure

Thermogravimetry (TGA) is an analysis technique in which the mass of a substance is measured as a function of temperature, while the substance is subjected to a controlled temperature program [25]. The first tool for this analysis was developed by K. Honda in 1915, and it is, nowadays, one of the most exploited methods.

The results of this thermal analysis (i.e. thermogram), can be presented as [27]:

- **Thermogravimetric curve:** normalized weight plotted as function of temperature or time (Figure 4)
- **Differential thermogravimetric curve:** rate of weight loss plotted as function of temperature or time (Figure 5).

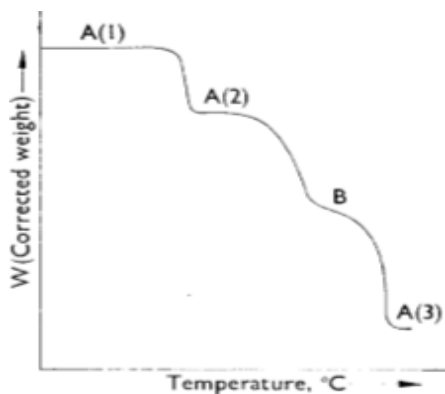


Figure 4. Example of thermogravimetric curve [27]

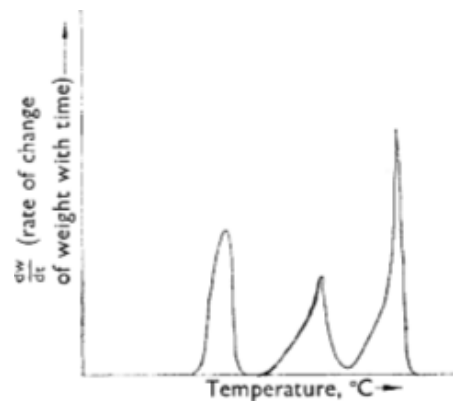


Figure 5. Example of differential thermogravimetric curve [27]

In the above shown plot the main features of thermogravimetric curve can be identified:

- A horizontal plateau in TG curve corresponding to a constant weight, where no mass loss (related to reaction or volatile release) takes place
- A curved portion in TG curve corresponding to a peak in DTG, which indicate the maximum degradation rate
- A non-null minimum in the DTG curve that may imply the simultaneity of two reactions and, therefore, the formation of an intermediate compound. The value of such a point allows to measure the stability of the intermediate compound and the extent of reactions overlapping.

Differential thermogravimetric curves allow to evaluate the reaction mechanism as each peak (or shoulder) is characteristic of a single reaction [28], hence, their number and height describes respectively degradation steps and reaction rates.

One of the main problems of this kind of thermal analysis is its strong dependency from many test variables, especially the heating rate. Moreover, as Guiochon et al. pinpointed in their work [29], this value of temperature is neither a true decomposition temperature (i.e.

initiation temperature) nor a transition temperature but can be considered as a “procedural decomposition temperature” [30].

Still, this value has been proven to be useful. Pellon et al. [31] in their work, for instance, uses a value of temperature  $T_{10}$ , at which the weight change is 10%, as a tool to assess thermal stability.

As mentioned, several factors influence the shape of a thermogram for a particular compound, among which the most important are:

- Heating rate ( $\beta$ ): For a single-stage reaction, the following relations have been demonstrated [32,33,34]:
  - I.  $(T_f)_{fast} > (T_f)_{slow}$
  - II.  $(T_i)_{fast} > (T_i)_{slow}$
  - III.  $(T_f - T_i)_{fast} > (T_f - T_i)_{slow}$

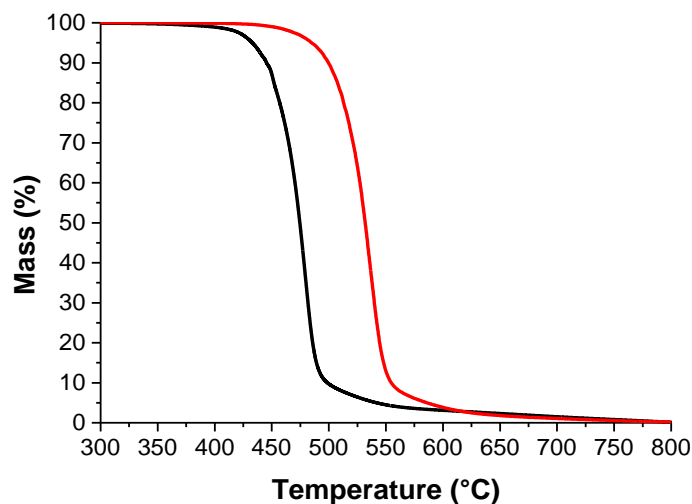


Figure 6. Example of polycarbonate thermograms obtained for low (black) and high heating rate (red)

Where  $T_f$  and  $T_i$  are, respectively the temperature at which the degradation reaction is completed and the procedural decomposition temperature, while the subscripts “fast” and “slow” indicate the heating rate. Moreover, Newkirk et al. [30], showed that, the extent of degradation reaction decreases at higher  $\beta$  at any temperature.

Further, slower heating rates allow a clearer separation between DTG peaks and, therefore, grant the dissociation of two subsequent reactions.

- Sample mass, volume and thermal properties: Thermogravimetric curves can be affected by sample mass and volume in three ways:
  - I. Temperature gradients within the material due to slow heat diffusion, which can lead to non-homogeneous reaction kinetic. This effect is particularly marked in substances characterized by low thermal conductivity.

- II. Temperature gradients due to exo- or endothermic reactions within the sample, deviating local temperature from the programmed linear increasing one.
- III. Limited diffusion of gas both environmental (e.g. oxygen) and produced by the thermal activated reaction.

The standard recommends a sample mass in the range of 1-10 mg: a smaller mass would not allow to obtain a reliable signal, while a bigger one would bring as well to a non-determined signal due to non-homogeneous condition (i.e. temperatures, gas concentration). In this project, has been used an average mass of  $10 \pm 0.5$  mg.

Several studies have been performed on the effect of different mass and surfaces [35,36,37]. They pinpointed that the state of subdivision is crucial in order to perform TG analysis, in particular, a lower extent of decomposition has been observed for samples of bigger size.

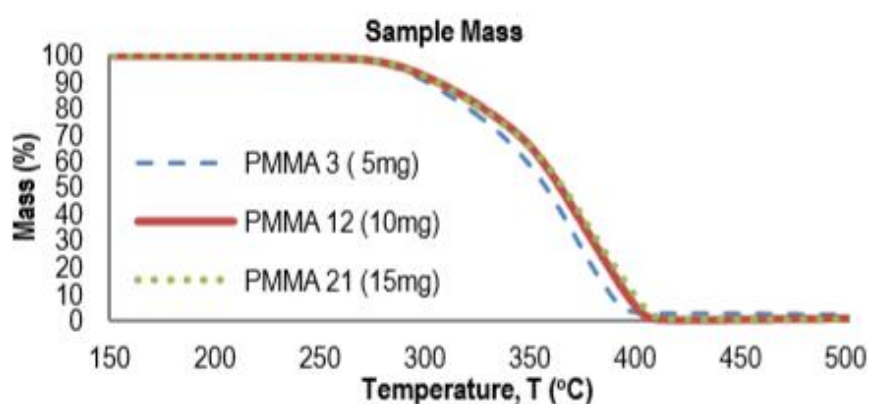


Figure 7. Example of PMMA thermograms obtained for samples with different mass [97]

- Atmosphere: environmental gas can affect thermogram differently according to its reactivity with the sample (Figures 8 and 9):
  - I. Inert gas with respect to sample: the role of the gas is merely to preserve an almost constant atmosphere around the sample throughout the test by removing gaseous reaction products [38], for this reason it does not affect the TGA result.
  - II. Reactive gas (e.g. oxygen): it modifies drastically the shape of the thermogravimetric curve, as the degradation reaction involves different species and may follow different kinetic. This may result, moreover, in the presence of supplementary peaks in DTG curve.

The essential instrumentation required is:

- A thermo-balance composed of a furnace to provide controlled heating rates, a high precision continuously recording balance (sensitivity of  $\pm 10 \mu\text{g}$ ), a temperature sensor, a system for the control of atmosphere (99.9% pure inert or reactive gas)
- A temperature controller capable of reach and maintain selected thermal program with a maximum error of  $\pm 0.1 \text{ }^\circ\text{C}$

- A recording device able to express the mass loss as a function of time and temperature
- A suitable gravimetrically stable container (e.g. crucible) that must be inert with respect to the test material.

Experimental tests can be performed with two different applied thermal history: simple ramp from room temperature to selected end point (i.e. 600°C) or with an underlying temperature modulation. In this work only simple ramp test were performed.

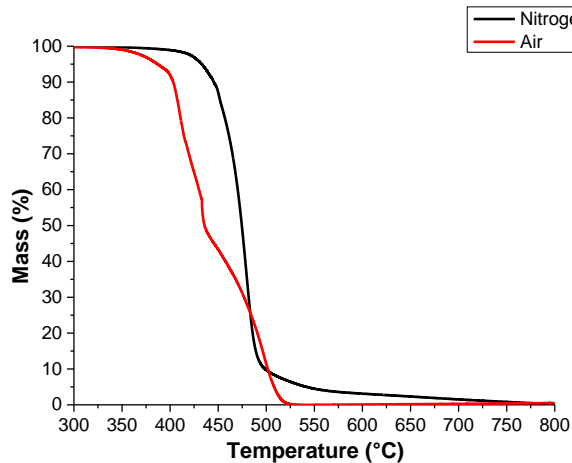


Figure 8. Example of thermograms obtained in air (red) and N<sub>2</sub> atmosphere (black) for polycarbonate

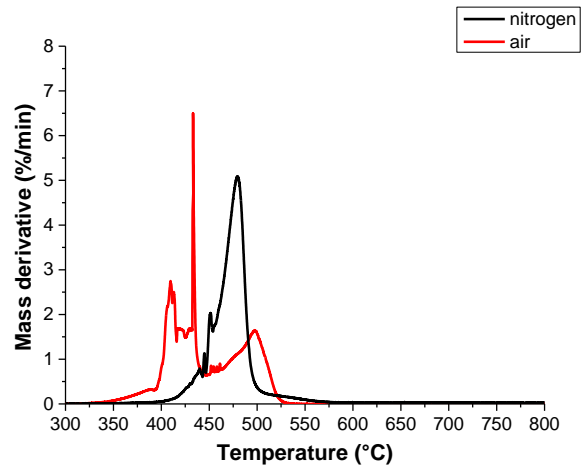
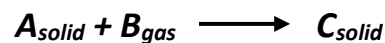


Figure 9. Example of DTG obtained in air (red) and N<sub>2</sub> atmosphere (black) for polycarbonate

### 1.2.1.2 Kinetic parameters

For some classes of reaction (below), thermogravimetric results can be exploited to estimate the reaction kinetics, more precisely a quantity called “thermal endurance” and “thermal index”, which is defined as the time-to-failure of a certain material subjected to a constant temperature field. This parameter is strictly related to another quantity called “thermal index”, which, instead, describes the maximum temperature that a material can withstand in order to accomplish the whole duration of a defined service life.



Such a method provides several advantages with respect to conventional isothermal studies like the lower amount of required data and time and the evaluation within a range of temperatures.

Several approaches have been proposed, that can be divided in two main classes: model-free and model-based methods. The first class, as suggested by its name, does not require a preliminary assessment of the involved reactions during the degradation process, but its lack

of precision limits the employability. On the other hand, model-based methods present higher precision, but their use is limited by a correct reaction evaluation.

A complete description of thermally activated reactions aims at developing a model that can be applied for any thermal treatment, regardless the applied thermal history [39,40]. Due to the high variety of reactions that could affect different materials, most researchers used several simplifying approximations. The most exploited one, found in many different papers [81,82,83], is the assumption that the transformation rate during a reaction is the product of two functions, one depending solely on the temperature (T) and the other depending solely on the fraction transformed ( $\alpha$ ):

$$\frac{d\alpha}{dt} = f(\alpha)k(T) \quad (\text{Eq. 1})$$

Where  $k(T)$  is the kinetic constant assumed to follow an Arrhenius type dependency:

$$k(T) = A \exp\left(-\frac{E}{RT}\right) \quad (\text{Eq. 2})$$

While  $f(\alpha)$  is a function depending on the degradation reaction type, estimated by mean of other analyses. Different formulations for various reactions are summarized in Table 2.

Mechanism	$f(\alpha)$
First order	$1 - \alpha$
Second order	$(1 - \alpha)^2$
Third order	$(1 - \alpha)^3$
One-dimensional diffusion	$(2\alpha)^{-1}$
Two-dimensional diffusion	$[-\ln(1 - \alpha)]^{-1}$
Power law	$2\alpha^{1/2}$
Avrami-Erofe'ev	$2(1 - \alpha)[- \ln(1 - \alpha)]^{1/2}$
Contracting area	$2(1 - \alpha)^{1/2}$
Contracting volume	$3(1 - \alpha)^{2/3}$

Table 2. Algebraic expression of  $f(\alpha)$  for most common reaction mechanisms operating in solid-phase reactions [39]

For thermogravimetric analysis performed at constant heating rate ( $\beta$ ) and considering Equation 2, it is possible to rewrite Equation 1 as:

$$\frac{d\alpha}{dt} = \frac{d\alpha}{dT} \frac{dT}{dt} = \frac{d\alpha}{dT} \beta = Af(\alpha) \exp\left(-\frac{E}{RT}\right) \quad (\text{Eq. 3})$$

In order to estimate Arrhenius activation energy (E) from Equation 3, different approaches may be exploited, among which Ozawa-Flynn-Wall and Kissinger methods are the most used.

## Ozawa-Flynn-Wall method

Ozawa-Flynn-Wall [85] method is a model-free description of activation energy that is based on the general rate equation (Equation 1). It is characterized by two main assumption:

- activation energy is considered as a function of conversion ( $\alpha$ ) alone
- reaction kinetic is assumed to be of the first order, which is typical of a random scission propagation reaction.

Therefore, according to Table 2, Equation 3 becomes:

$$\frac{d\alpha}{dT} = A(1 - \alpha) \exp\left(-\frac{E}{RT}\right) \frac{1}{\beta} \quad (\text{Eq. 4})$$

Integrating Equation 4, a direct correlation between conversion and temperature can be obtained:

$$\int_0^{\bar{\alpha}} \frac{d\alpha}{(1 - \alpha)} = \frac{A}{\beta} \int_{\tau_0}^{\tau} \exp\left(-\frac{E}{RT}\right) dT \quad (\text{Eq. 5})$$

Where  $\bar{\alpha}$  is the conversion percentage related to temperature  $\tau$  and  $\tau_0$  is the initial temperature. The integral in the right part of the equation cannot be solved analytically, as it gives:

$$\int_{\tau_0}^{\tau} \exp\left(-\frac{E}{RT}\right) dT = \frac{E}{R} \left( \frac{\exp\left(-\frac{E}{RT}\right)}{\frac{E}{RT}} + Ei\left(-\frac{E}{RT}\right) \right) = \frac{E}{R} p\left(-\frac{E}{RT}\right) \quad (\text{Eq. 6})$$

Where  $Ei(-E/RT)$  is a non-elementary function, called exponential integral function, that can be evaluated only by means of approximated numerical methods. Lots of function can be used to determine the polynomial  $p(-E/RT)$ , depending on their applicability ranges and desired precision. For what concerns the investigated process, Doyle equation [63] has been proven to be one of the most reliable models.

It is expressed as:

$$\log\left(p\left(-\frac{E}{RT}\right)\right) = -2.315 - 0.457 \left(\frac{E}{RT}\right) \quad (\text{Eq. 7})$$

$$20 \leq \frac{E}{RT} \leq 65$$

By combining Equations 5, 6 and 7 and taking the logarithm of the resulting equation, the final conversion-temperature relation can be obtained:

$$\log(\ln(1 - \bar{\alpha})) = \log\left(\frac{AE}{R}\right) - \log(\beta) - 2.315 - 0.457 \left(\frac{E}{RT}\right) \quad (\text{Eq. 8})$$

It can be noticed that, for a constant conversion, Equation 8 can be written in form of a straight-line (i.e.  $y=mx+q$ ), with  $\log(\beta)$  on the y-axis and  $1/T$  on the x-axis. Hence:

$$q = -\log(\ln(1 - \bar{\alpha})) + \log\left(\frac{AE}{R}\right) - 2.315 \quad (\text{Eq. 9})$$

$$m = \frac{d \log(\beta)}{d \frac{1}{T}} = -0.457 \left(\frac{E}{R}\right) \quad (\text{Eq. 10})$$

As it can be seen, Equation 10 provides an estimation of the activation energy for the degradation reaction, that can be calculated as:

$$E = \frac{R}{b} \left( \frac{d \log(\beta)}{d \frac{1}{T}} \right) \quad (\text{Eq. 11})$$

where  $b$  is a parameter called Doyle's constant: a correction parameter that will be explained in next chapter.

Even if it is not useful for thermal endurance and activation energy estimation, the model offers two equations for the calculation of the pre-exponential factor ( $A$ ). The first is derived from Equation 8 by substituting heating rate ( $\beta$ ), temperature ( $T$ ) and activation energy ( $E$ ) values:

$$A = 10^{2.315 + 0.457 \left(\frac{E}{RT}\right)} \left(-\frac{\beta R}{E}\right) \ln(1 - \alpha) \quad (\text{Eq. 12})$$

The second one is based on Doyle's approximation and depends on a second constant ( $a$ ) and is expressed as:

$$A = 10^a \left(-\frac{\beta R}{E}\right) \ln(1 - \alpha) \quad (\text{Eq. 13})$$

Comparing Equations 12 and 13, it can be noticed that the value  $a$  is related with the Doyle's equation (i.e.  $p\left(-\frac{E}{RT}\right)$ ), in particular:

$$a = -p\left(-\frac{E}{RT}\right) = 2.315 + 0.457 \left(\frac{E}{RT}\right) \quad (\text{Eq. 14})$$

After activation energy has been estimated for different degree of degradation, it is possible to move on to the derivation of thermal endurance and thermal index.

The starting point is a modified form of Equation 3, which is here described as a function of sample weight ( $w$ ) instead of degree of conversion ( $\alpha$ ). Moreover, it can be noticed that sample weight and conversion percentage have opposite trend, therefore Equation 3 becomes:

$$\frac{dw}{dt} = -A f(w) \exp\left(-\frac{E}{RT}\right) \quad (\text{Eq. 15})$$

$$\frac{dw}{dT} \beta = -A f(w) \exp\left(-\frac{E}{RT}\right) \quad (\text{Eq. 16})$$

Where  $E$  is the activation energy estimated in the previous paragraph.

Solving these differential equations, the following can be derived:

$$t_f = \int_0^{t_f} dt = -\exp\left(\frac{E}{RT}\right) \int_{w_0}^{w_f} \frac{1}{Af(w)} dw \quad (\text{Eq. 17})$$

$$\int_{w_0}^{w_f} \frac{1}{Af(w)} dw = -\frac{1}{\beta} \int_{T_0}^{T_f} \exp\left(\frac{E}{RT}\right) dT \quad (\text{Eq. 18})$$

where  $t_f$  is the polymer service life for the selected failure criterion in isothermal condition.

Combining Equation 17 and 18, a more convenient formulation can be obtained:

$$t_f = \frac{1}{\beta} \exp\left(\frac{E}{RT}\right) \int_{T_0}^{T_f} \exp\left(\frac{E}{RT}\right) dT \quad (\text{Eq. 19})$$

As for Equation 7, it cannot be solved analytically, but requires an approximated numerical method. By adopting Doyle's approximation (i.e. Equations 7 and 13), an estimation of the thermal endurance can be provided:

$$\log(t_f) = \frac{E}{RT \ln(10)} + \log\left(\frac{E}{R\beta}\right) - 2.315 - 0.457 \left(\frac{E}{RT}\right) \quad (\text{Eq. 20})$$

$$\log(t_f) = \frac{E}{RT \ln(10)} + \log\left(\frac{E}{R\beta}\right) - a \quad (\text{Eq. 21})$$

This formulation, hence, allows to estimate the failure time under known isothermal condition ( $T$ ) for fixed degree of degradation ( $\alpha$ ).

Being an approximated model, an assessment of the accuracy has to be provided, in particular a computational model for standard deviation is provided:

$$\frac{\sigma t_f}{t_f} = \left(1 - 0.052 \frac{E}{RT}\right) \left(\frac{\sigma E}{E}\right) \quad (\text{Eq. 22})$$

Moreover, by reversing Equation 21, the thermal index can be evaluated:

$$TI = \frac{E}{R \ln(10) \left[ \log(t_f) - \log\left(\frac{E}{R\beta}\right) + a \right]} \quad (\text{Eq. 23})$$

Differently from thermal endurance, thermal index provides an estimation of the isothermal condition (i.e. temperature value) for which the material reaches the degree of degradation ( $\alpha$ ) in an arbitrary selected time.

As for thermal endurance, it is possible to estimate thermal index standard deviation:

$$\frac{\sigma TI}{TI} = 1.2 \frac{\sigma E}{E} \quad (\text{Eq. 24})$$

The method, moreover, offers a system for the calculation of the process reaction order by performing an isothermal thermogravimetric analysis. The formulation can be derived from Equation 3 with the assumption of constant temperature:

$$n = \frac{d \ln\left(\frac{d\alpha}{dt}\right)}{d \ln(1 - \alpha)} \quad (\text{Eq. 25})$$

This method has been standardized in ASTM E1641 [89] and E1877 [90] and in ISO 11358 [91], the latter being characterized by non-application of Doyle correction factor.

Despite the mathematical approximations considered in determination of the integral of Equation 3, this method provides good results [42,43], even though some limitations have been highlighted.

Brems et al. [44] in their work on polystyrene (PS) and polyethylene-terephthalate (PET) pyrolysis showed a good result accuracy for first and second order kinetics, even though high activation energy variations have been recorded for heating rates lower than 1°C/min.

Baroni et al. studies [45], moreover, described isoconversional models as an initial step to the modeling of thermal decomposition, which has to be improved for polymers presenting more than one degradation step (i.e. more than one peak in DTG curve)

Nevertheless, simulations performed on biomass samples showed that the kinetic parameters calculated with Ozawa–Flynn–Wall model presented a rather satisfactory agreement with experimental data.

Several researches have been performed in order to expand OFW applicability field.

D. R. Dowdy [46] in his work introduced a new instantaneous activation energy parameter in order to study degradation phenomena characterized by multiple simultaneous reactions. It is defined as an average  $E_a$  for reactions that occurs at a given instant and have the following formulation:

$$E_{inst} = \frac{\sum \left(\frac{d\alpha}{dt}\right)_i E_i}{\sum \left(\frac{d\alpha}{dt}\right)_i} \quad (\text{Eq. 26})$$

where  $E_i$  is the activation energy and  $(dC/dt)_i$  is the conversion rate of the single reaction.

This method has been proven to be valid for independent reactions, while present some limitations for competitive ones.

Further, Celina et al. [47] in their review highlighted main deficiencies of OFW approach for the estimation of kinetic parameters and service life:

- i) Diffusion limiting oxidation (DLO) process cannot be avoided in thermogravimetry performed in  $O_2$  rich environment. For this reason, resulting thermograms are not accurate representation for oxidation kinetic, which is highly affected from polymer diffusion coefficient and mass.
- ii) Arrhenius linear behavior is generally observed solely within a certain temperature range, leading to an overestimation of activation energy values for degradation process at too high and too low temperatures.
- iii) The enhanced material volatilization operated by thermogravimetric analysis may hinder some thermo-oxidative reactions. Some polymers, indeed, tend to increase their weight due to oxygen absorption.

## Kissinger method

Differently from OFW, this method is not based on an approximated solution of Arrhenius integral, but exploits differential thermogravimetric analysis. In particular, it provides an estimation of activation energy by extrapolating the temperature of maximum reaction rate ( $T_{max}$ ), which corresponds to the peak temperature in DTG plot.

It can be expressed as:

$$E = R \frac{d \ln \left( \frac{\beta}{T_{max}^2} \right)}{d \left( \frac{1}{T_{max}} \right)} \quad (\text{Eq. 27})$$

Kissinger method is the simplest and most suitable way to estimate kinetic parameter for degradation of pure compounds and, moreover, can be applicable for the study of some more complex reaction, e.g. biomass degradation [41].

On the other hand, as described by Slopeicka [48] and Kongkaew [49] in their works, activation energy estimated with this method does not vary during pyrolysis process and, therefore, does not reveal complex reaction mechanism that are otherwise reported by OFW method.

### 1.2.2 Long-term analysis

It is possible to estimate thermal index by studying decay of a particular set of material properties due to the applied temperature field. In this case thermal index provides an indication of material's ability to retain a specific property over time when exposed to elevated temperatures.

Standard UL 746B [75] describes mathematical procedure for TI estimation and a set of three tests selected in order to simulate the field-service conditions as closely as possible. In particular, for polymeric materials, examined properties are tensile, impact and dielectric strength, whose variation is plotted as a function of logarithm of time (Figure 10).

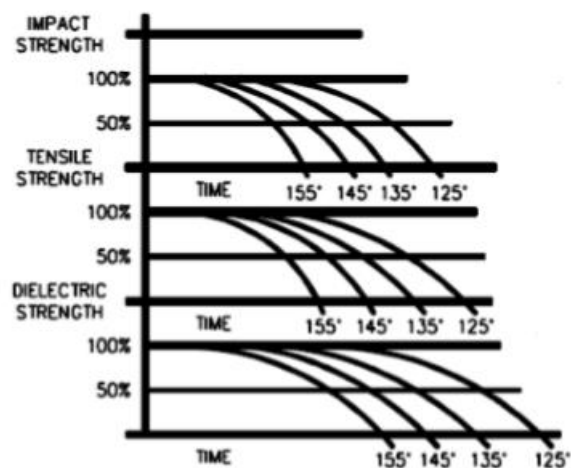


Figure 10. Representative plot of impact, tensile and dielectric strength decay over time for a specimen subjected to constant temperature field [75]

Failure times ( $t_f$ ), estimated by selecting a suitable failure criterion (e.g. 50% loss of property), are then related to temperature by mean of Arrhenius equation (Equation 28):

$$\ln(t_f) = -\frac{E}{R} \frac{1}{T} + \ln(A) \quad (\text{Eq. 28})$$

By plotting the logarithm of failure time as a function of reciprocal temperature and performing a linear regression, it is possible to estimate the activation energy (E) and the Arrhenius pre-exponential factor (A). At this point, by reverting Equation 28, the thermal index can be calculated as:

$$\text{Thermal index} = T = \frac{-E}{R(\ln(t_f) - \ln(A))} \quad (\text{Eq. 29})$$

It has to be highlighted that this procedure is highly dependent on sample shape, hence, in order to determine the above mentioned properties, the use of standardized specimen with high exposed surface is highly suggested.

This methodology offers, generally, a similar thermal index value with respect to thermogravimetric analysis, although, the lower amount of time and tests required for a complete assessment makes TGA method more appreciable for practical use [76].

### 1.2.3 Differential thermal analysis (DTA)

Differential thermal analysis (DTA) is a technique in which the temperature difference ( $\Delta T$ ) between a substance and a reference material is measured, while they are subjected to the same controlled heating program [50]. By plotting  $\Delta T$  as a function of temperature a graph like the one showed in Figure 11 is obtained.

The observed positive peak indicates the occurrence of an exothermic process in the sample, e.g. oxidation; vice versa, negative peaks are characteristic of the endothermal one, e.g. melting.

Enthalpy change ( $\Delta H$ ) related to the thermal event can be estimated from DTA plot by the following relation:

$$\Delta H = \frac{A}{K m} \quad (\text{Eq. 30})$$

where m is the sample mass, A is the area defined by the peak and the base line and K is the calibration factor.

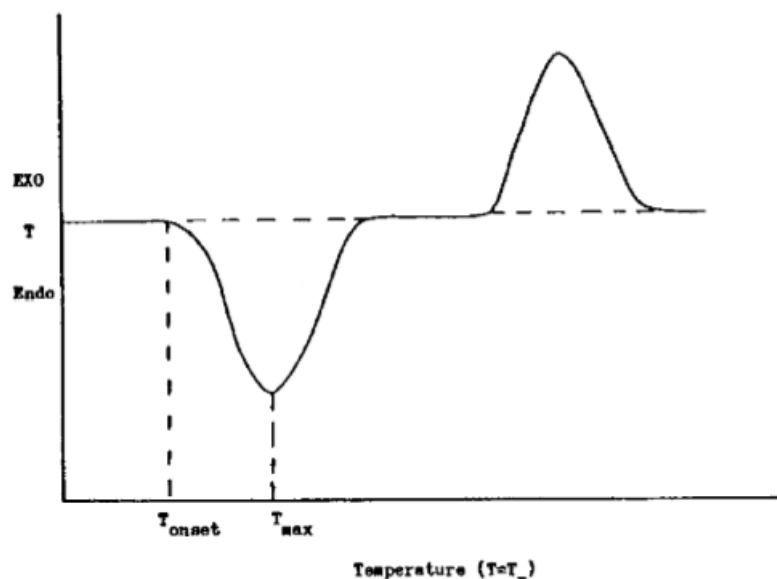


Figure 11. Example of differential thermal analysis plot

This factor can be computed by mean of Equation 30 by relating the measured area to a known enthalpy change; generally, the melting process of pure metal such as indium is used. Calibration factor is strongly dependent on reference material, whose thermal properties (e.g. conductivity) should be constant and comparable to sample's ones throughout the whole process [51].

A schematic representation of the apparatus is provided in figure 12.

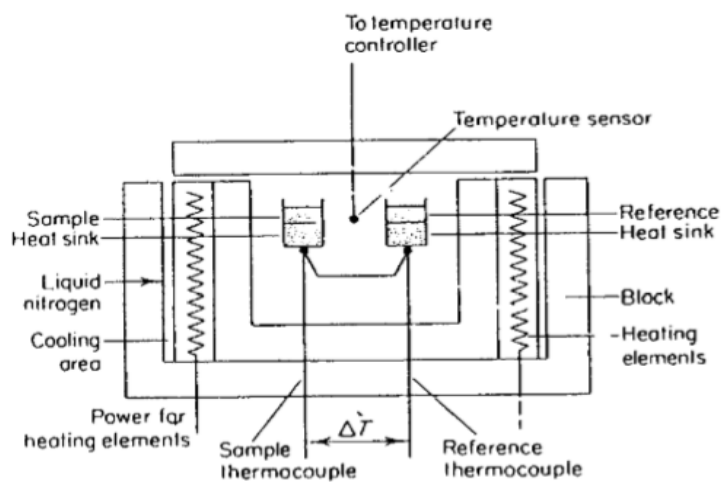


Figure 12. Schematic representation of DTA apparatus

As for thermogravimetry, DTA graph is strongly affected by several parameters [52]:

- Heating rate ( $\beta$ ): determines the shape of the peaks. The use of low  $\beta$  value is suggested in order to achieve a good separation between the peaks.
- Atmosphere: gas-sample reactivity varies the reaction mechanism, leading to an alteration in peaks number and position.

- Thermo-mechanical history: the presence of undesired residual stresses leads to the appearance of a corresponding peak.
- Presence of volatile substances within the sample

As demonstrated by Boersma et al. [53], classical DTA cannot be exploited for quantitative measurement because of the temperature gradient within the sample, which leads to non-homogeneous behavior.

In order to settle this problem, the original apparatus have been modified [54] by moving thermocouple junction outside the sample and inserting a heat flux estimator between sample and furnace. DTA analyses performed with this apparatus is generally known as heat-flux differential scanning calorimetry (hf-DSC).

DTA technique is mainly used for determination of characteristic temperature such as glass transition ( $T_g$ ), melting ( $T_m$ ) and decomposition ( $T_d$ ), although, it can be exploited for estimation of particular heats (e.g. fusion, vaporization, reaction, crystallization) and process activation energy.

### 1.2.4 Differential scanning calorimetry (DSC)

Differential scanning calorimetry (DSC) is a technique developed from DTA, in which the sample and a reference material, connected to different heating systems, are kept to the same temperature throughout a controlled heating (or cooling) rate [55]. The resulting thermogram (Figure 13) is obtained by plotting the difference in supplied power among the heating system as a function of temperature.

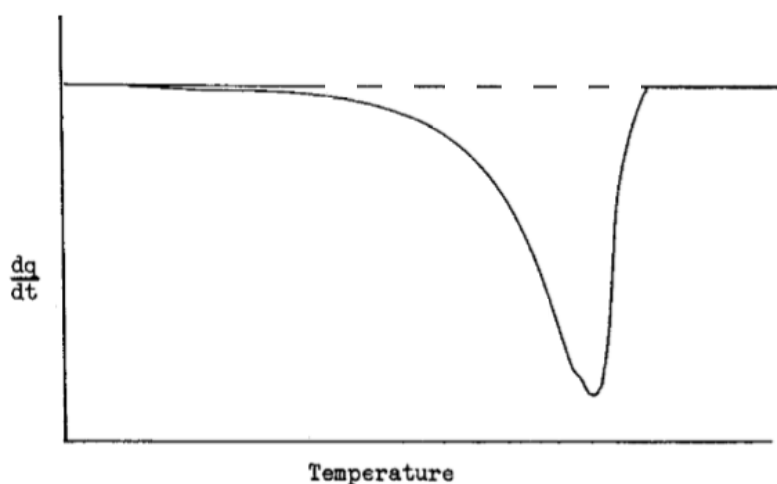


Figure 13. Example of differential scanning calorimetry thermogram [55]

As for DTA analysis, heat induced process are described as positive or negative deviation from the baseline and the relative enthalpy change can be derived from Equation 30, although,  $K$  does not depend on temperature and, therefore, allowing a faster calibration procedure.

The effect of process parameter on this technique is analogous to the one observed for DTA.

The device exploited for DSC analyses is schematically represented in Figure 14.

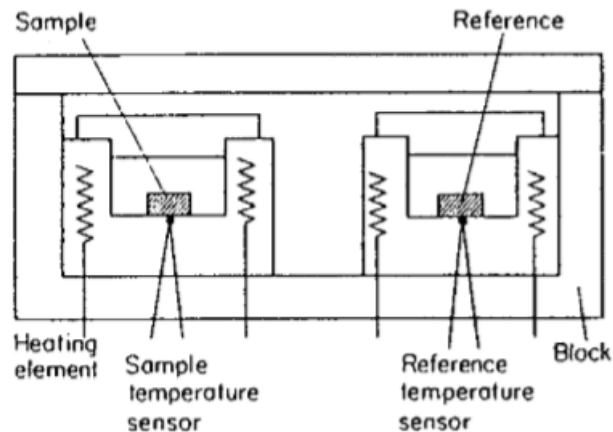


Figure 14. Schematic representation of differential scanning calorimetry apparatus

According to Blaine [56] and Perkin [54] work, heat-flux DSC and DSC can be considered equivalent for what concerns the information obtained by result analysis, even though, differential scanning calorimetry cannot be applied for the study of phenomena occurring at temperature values higher than 700°C.

Differential scanning calorimetry analysis meets several practical applications for estimation of parameters such as apparent heat capacity, thermal stability, crystallization kinetic and transition temperatures [52]. Moreover, it can be used for monitoring the curing period of thermosetting polymers [51].

In conclusion, DSC allows to estimate, with low degree of accuracy, process kinetic parameter, such as reaction rate, activation energy, reaction order, preexponential factor.

### 1.3 Purpose of work

Polymer processing is generally characterized by a complex combination of aggressive conditions, which can lead to material degradation followed by a reduction in properties value with respect to the raw material. Hence, an assessment of degradative behavior of material subjected to different environmental condition may provide a better control over processing, leading to a quality increase of final product.

This project presents two main goals. The first is the evaluation of polymer degradation caused by high temperatures, reaction with environmental gasses (i.e. oxygen) and mechanical stress by mean of different analysis methods. The second is a verification of applicability field Ozawa-Flynn-Wall method for the estimation of kinetic parameters of degradation process.

Thermal endurance and relative conditions of validity have been evaluated for thermal and thermo-oxidative degradation by mean of thermogravimetric analysis using Ozawa-Flynn-Wall method. Effect of shear stress on melt polymer, instead, has been determined form the extent of molecular weight decrease, which have been obtained by mean of viscosity measurements, i.e. melt flow index and intrinsic viscosity.

Experimental tests have been performed on two materials characterized by a simple (i.e. polystyrene) and complex degradation process (i.e. polycarbonate).

Moreover, the effect of polymer molecular weight have been studied by comparison of kinetic parameters obtained for two types of polystyrene, PS N2982 and PS N2380.



## 2. Materials and methods

### 2.1. Materials

The analysis presented in this work were performed on three different materials, namely polystyrene N2982, polystyrene N2380 and high-density polyethylene. The raw materials were provided in form of non-charged pellets with an average weight of  $20 \pm 5$  mg per granule.

#### 2.1.1 High-density polyethylene

High-density polyethylene (HDPE) is a low cost thermoplastic semicrystalline polymer presenting a linear molecular structure. It is produced by free radical polymerization with the addition of a Ziegler-Natta or a Phillips-type catalyst.

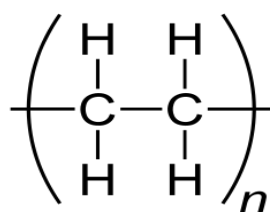


Figure 15. Molecular structure of polyethylene

It is characterized by a glass transition temperature of  $110^{\circ}\text{C}$ , a melting temperature of  $130^{\circ}\text{C}$  and a crystallinity of 70-90%. The typical processing temperatures depend on the type of polystyrene and generally are  $180\text{-}205^{\circ}\text{C}$  for extrusion and  $200\text{-}250^{\circ}\text{C}$  for injection moulding (mould temperature =  $20\text{-}95^{\circ}\text{C}$ ).

HDPE is a strong, high density, moderately stiff plastic and is one of the most widely used polymers, with an average annual production of around 30 million of tonnes. Its characteristics and low cost make HDPE suitable for several applications in various field, among which the main ones are:

- Food and beverage container which does not contaminate edible products
- Toys resistant to damaging and discoloring
- Chemical container due to its low reactivity with the majority of common solvents
- Pipe system

Thermal degradation phenomena affecting this material can be described by the mechanisms derived by Flory for polymerization of polyolefins [77], which is a radical chain reaction.

It has been proven [78] that HDPE degradation initiation occurs at around  $360^{\circ}\text{C}$  and is mainly driven by random chain scission. Propagation phenomena mechanism, furthermore, consists of inter- and intramolecular hydrogen abstraction, which can lead to crosslink formation and volatilization of oligomers, respectively [79].

Finally, termination reaction can be mainly identified as disproportionation, where two radicals come together to form an alkane and an olefin [80].

### 2.1.2 Polystyrene N2982 & N2380

Polystyrene (PS) is an inexpensive thermoplastic amorphous polymer presenting a linear molecular structure. It can be produced by anionic or free radical polymerization, generally, with the addition of a catalyst.

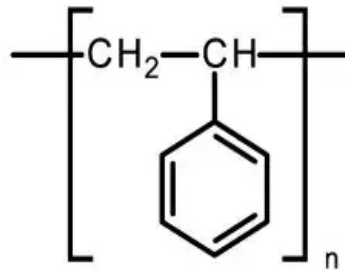


Figure 16. Molecular structure of polystyrene

It is characterized by a glass transition temperature in the range of 91-128°C, while do not show any melting one due to absence of crystallinity. The typical processing temperatures depend on molecular weight and generally are 190- 240°C for extrusion and 220-270°C for injection moulding (mould temperature = 20-60°C) [87].

Polystyrene can be produced in form of a solid (i.e. general-purpose polystyrene) or foamed (i.e. expanded polystyrene) and is one of the most widely used polymers, with an average annual production of several millions of tonnes. The material is transparent, insulating, hygienic, glossy, durable, sturdy, easy to process and flexible, features that make PS eligible to be used for a wide range of applications. As a matter of fact, it is mainly used in construction industry for roofing and plumbing, due to its high heat capacity and low cost, and for shatterproof and hygienic packaging [86].

In this work were studied two kind of polystyrenes: PS N2982 (low molecular weight) and PS N2380 (high molecular weight).

Polystyrene degradation has been exhaustively studied in the past years and, nowadays, a description of its mechanism can be provided.

The thermal degradation of polystyrene is characterized by a radical chain process which includes initiation, propagation, transfer and termination steps [56]. The degradation process is, therefore, composed of several competitive elementary reactions; the main ones are reported below (Table 3).

<i>Elementary reaction</i>	<i>Chain Reaction Step</i>	<i>Mode</i>
$\beta$ -Scission	Propagation	Depolymerisation Chain scission
Hydrogen abstraction	Transfer	Intramolecular: back-biting Intermolecular
Mutual destruction	Termination	Coupling Disproportionation (Evaporation)
C—C scission	Initiation	Weak points Chain end Random

Table 3. Main reactions of radical chain scission degradation process [56]

The dominant reaction is the so-called  $\beta$ -scission (Figure 17), which mainly involves chain end radicals and causes depolymerization which produces styrene, which is by far the most important volatile product (i.e.  $\approx 50\%$  of the total volatile product). However, under a threshold temperature ( $T_{th}=320^{\circ}\text{C}$ ) depropagation reaction is faster than propagation one, hence, no styrene production is observed [56].

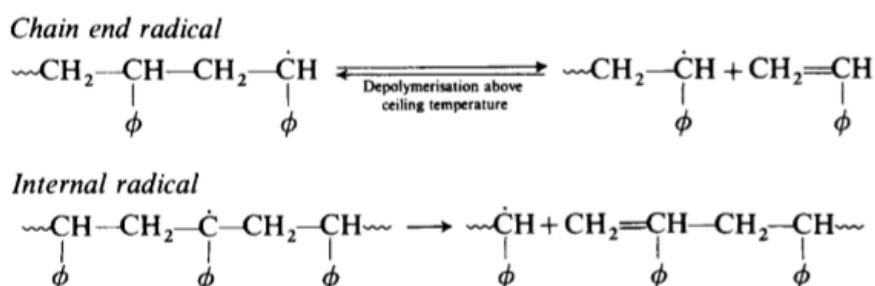


Figure 17.  $\beta$ -scission reactions

Moreover,  $\beta$ -scission reaction, coupled with chain transfer, can lead to formation of internal radical, bringing to chain scission and, therefore, to decrease of molecular weight and formation of an unsaturated chain end which is a weak structure, i.e. possible initiation site.

Another significant reaction is given by the abstraction of hydrogen atoms in the main chain by mean of a radical species. The reaction (Figure 18) produces an unsaturated chain end in the site of the attacking radical and a new internal radical which will immediately undergo  $\beta$ -scission. As demonstrated by Cameron et al. [57], hydrogen abstraction reaction can take place both among two different chains (i.e. intermolecular) and within a chain (i.e. intramolecular).

This last case is generally known as back-biting reaction and is characterized by formation of volatile dimeric or trimeric fragments.

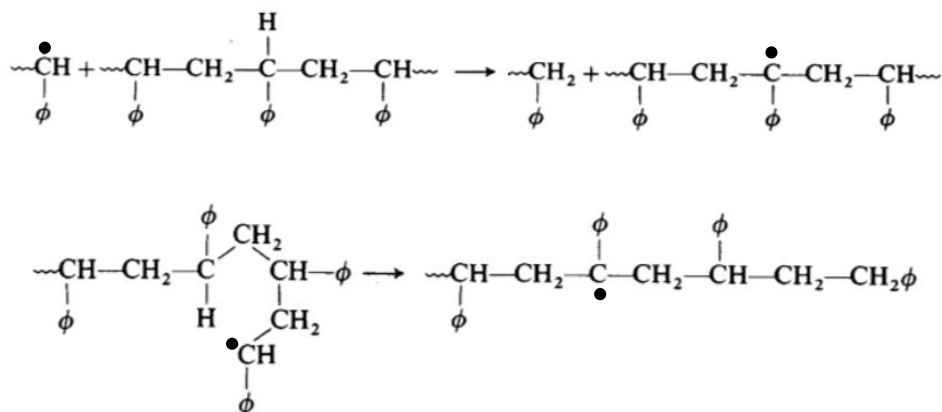


Figure 18. Intermolecular (above) and intramolecular (below) hydrogen abstraction reactions [58].

The initiation reaction can occur by random scission (see paragraph 1.1) or in sites characterized by weak links (e.g. defects). For this last reason, it has been noticed [58] that polystyrene produced by anionic polymerization have enhanced heat resistance with respect to the ones produced by radical polymerization.

The termination process presents a kinetic of the first order and have been proven [58] to take place through evaporation of small radicals.

For what concerns thermal-oxidation, Jellinek et al. [59] found that thermal degradation phenomena of polystyrene in the presence of oxygen can be described as hydroperoxide mechanism (see paragraph 1.1).

## 2.2 Thermogravimetric analysis

Thermogravimetric analyses were performed by following ASTM E2550 [88] by mean of a “TA Instruments Q500 thermogravimetric analyzer” characterized by a built-in results-oriented software and a balance characterized by a sensitivity of 0.1 mg and a weighing accuracy of  $\pm 0.01\%$ .

Samples were obtained cutting off pellets to an average weight of  $10 \pm 0.5$  mg.

The test were performed either in nitrogen or in air, and consisted in a heating ramp form room temperature to  $600^\circ\text{C}$ . The heating rate were  $1^\circ\text{C}/\text{min}$ ,  $2^\circ\text{C}/\text{min}$ ,  $3^\circ\text{C}/\text{min}$ ,  $5^\circ\text{C}/\text{min}$ ,  $7^\circ\text{C}/\text{min}$ ,  $10^\circ\text{C}/\text{min}$ ,  $15^\circ\text{C}/\text{min}$ , and  $20^\circ\text{C}/\text{min}$ .

As previously mentioned, obtained thermograms were studied by mean of ASTM E1641 [89] and ISO 113358 [91], which provide an estimation of the Arrhenius activation energy.

In order to apply Equation 11 for calculation of  $E_a$  a relation between heating rate and degradation temperature for a fixed conversion ( $\alpha$ ), must be found. The procedure consists in performing a set of thermogravimetric analysis at different heating rates (Figure 19) and extrapolate the degradation temperature for a fixed degree degradation (e.g.  $\alpha=40\%$ ).

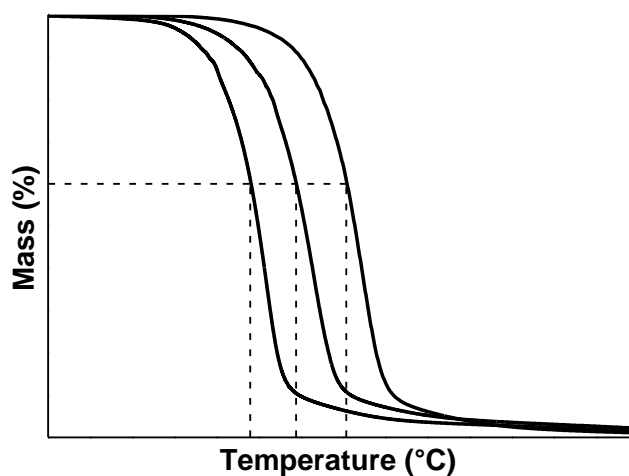


Figure 19. Example of thermogravimetric curves for different heating rates. The lowest one is one the left

Activation energies of the process can be estimated by plotting the logarithm of heating rates ( $\beta$ ) as a function of the reciprocal of isoconversional temperatures and by computing the linear regression (Figure 20).

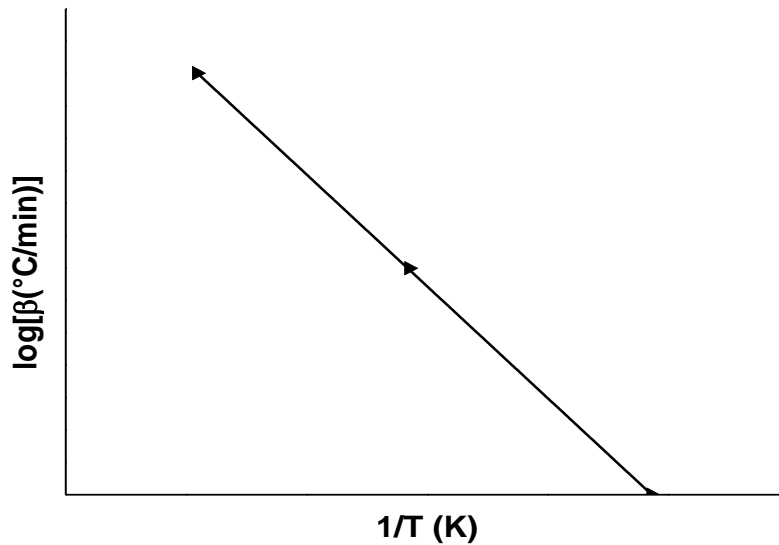


Figure 20. Example of experimental plot obtained using Equation 11

Even though a first estimation of activation energy is obtained, a further correction is necessary to obtain enhanced accuracy. In particular Doyle's constant (b) has to be modified according Table 4.

$E/RT_f$	a	b	$E/RT_f$	a	b	$E/RT_f$	a	b
8	5,3699	0,5398	26	14,1527	0,467	44	22,4148	0,454
9	5,898	0,5281	27	14,6187	0,466	45	22,8682	0,453
10	6,4157	0,5187	28	15,0836	0,465	46	23,3212	0,453
11	6,9276	0,511	29	15,5474	0,463	47	23,7738	0,453
12	7,4327	0,505	30	16,0103	0,4629	48	24,226	0,452
13	7,9323	0,5	31	16,4722	0,462	49	24,6779	0,452
14	8,4273	0,494	32	16,9333	0,461	50	25,1294	0,4515
15	8,9182	0,491	33	17,3936	0,461	51	25,5806	0,4511
16	9,4056	0,488	34	17,8532	0,459	52	26,0314	0,4508
17	9,89	0,484	35	18,312	0,459	53	26,482	0,4506
18	10,3716	0,482	36	18,7701	0,458	54	26,9323	0,4503
19	10,8507	0,479	37	19,2276	0,458	55	27,3823	0,45
20	11,3277	0,477	38	19,6845	0,456	56	27,8319	0,4498
21	11,8026	0,475	39	20,1408	0,456	57	28,2814	0,4495
22	12,2757	0,473	40	20,5966	0,4558	58	28,7305	0,4491
23	12,7471	0,471	41	21,0519	0,455	59	29,1794	0,4489
24	13,217	0,47	42	21,5066	0,455	60	29,6281	0,4487
25	13,6855	0,469	43	21,9609	0,454			

Table 4. Correlation between Doyle's constant and Doyle's equation argument

The refinement occurs by mean of an iterative process that is composed of three steps:

- Calculation of the value where  $T_f$  is the degradation temperature corresponding to the heating rate closest to the midpoint of all the heating rates
- Definition of the corresponding  $b$  value using data reported in Table 4
- Computation of Equation 11 with the new Doyle's constant

The procedure end when  $b$  no longer changes with the next iteration.

For what concerns the estimation of thermal endurance and thermal index, ASTM E1877 [90] suggest the use of a slightly different approximated method developed by Xu [64] in order to evaluate of integral in Equation 19:

$$\log \left( \int_{T_0}^{T_f} \exp \left( \frac{E}{RT} \right) dT \right) = -\log(100.4) - 0.463 \frac{E}{RT_f} \quad (\text{Eq. 31})$$

where  $T_f$  and  $E$  are the values of failure temperature and activation energy, respectively, derived by mean of the Ozawa-Flynn-Wall method.

Therefore, the corrected thermal endurance (Equation 32) and thermal index (Equation 33) can be determined:

$$\log(t_f) = \frac{E}{RT \ln(10)} + \log \left( \frac{E}{100.4R\beta} \right) - 0.463 \left( \frac{E}{RT_f} \right) \quad (\text{Eq. 32})$$

$$TI = \frac{E}{R \ln(10) \left[ \log(t_f) - \log \left( \frac{E}{100.4R\beta} \right) + 0.463 \frac{E}{RT_f} \right]} \quad (\text{Eq. 33})$$

It can be noticed that the service life formulation (Equation 32) is composed of three terms:

- the first considers the temperature at which the assessment has to be performed;
- the second analyze the effect of heating rate;
- the third deals with the failure temperature estimated from thermogravimetric curves;

For what concerns the accuracy evaluation, Xu proposed a complex method including additional experimental tests that will not be treated in here.

Skoog et al. [66], moreover, described a simpler accuracy evaluation method in the same form of Equations 22 and 24:

$$\frac{\sigma t_f}{t_f} = \ln(10) \log(t_f) \frac{\sigma E}{E} \quad (\text{Eq. 34})$$

$$\frac{\sigma TI}{TI} \approx \pm 0.19 \frac{\sigma E}{E} \quad (\text{Eq. 35})$$

An example of thermal endurance curve (Figure 21) is provided below for a general value of conversion ( $\bar{\alpha}$ ). It is important to notice that failure time ( $t_f$ ) is plotted in logarithmic scale, whereas temperature (T) is in linear scale.

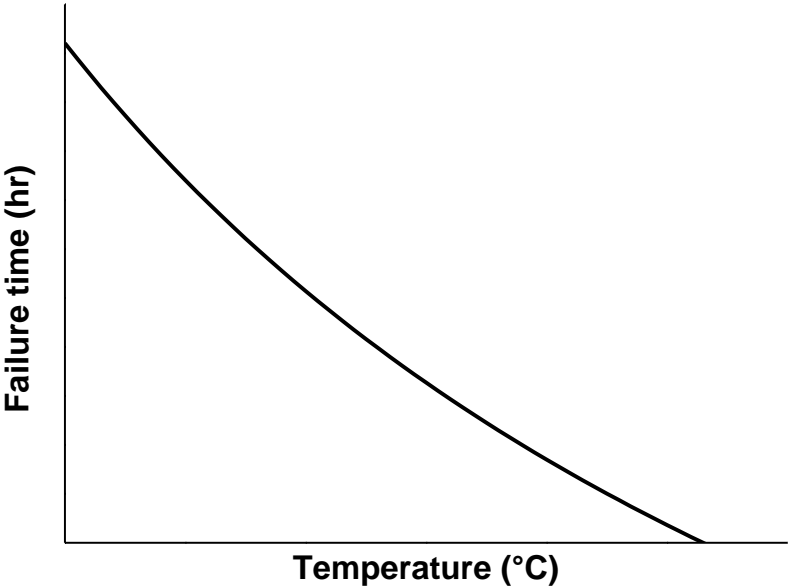


Figure 21. Example of thermal endurance curve

## 2.3. Molecular weight estimation

In this work polymer molecular weight has been evaluated by performing a viscosity evaluation, which can be related to  $M_w$  through some well-known methods (i.e. Mark-Houwink [92]).

Degradation reactions activated by heat and oxygen can be simply described as a reduction of molecular mass of a polymer, therefore, the estimation of this last parameter can be exploited for a more precise evaluation of reaction extent.

Polymer viscosity has been evaluated throughout this work by mean of two different techniques: melt flow index measurement and intrinsic viscosity determination.

### 2.3.1. Melt flow index

Melt flow index (MFI) or melt flow rate (MFR) is defined as the mass of melt polymer, in grams, that flows through a nozzle in 10 minutes due to a constant applied load under fixed temperature conditions. This quantity is generally extrapolated by weighting different subsequently cut thread by mean of the following equation:

$$MFI(T, m_{nom}) = \frac{m_{av}}{t_{cut-off}} \quad (\text{Eq. 35})$$

Where  $m_{av}$  is the average mass of the cut tread,  $t_{cut-off}$  is the time between two subsequent cuts.

It is not generally used for the quantitative estimation of molecular weight but provides just an indication about the flow characteristic of melt polymer. However, according to the work of Bremner [67], molar mass can be estimated from MFI for certain materials but, due to the lack of accuracy of this method, it was not used in this work. As a matter of facts, MFI is generally used just as qualitative analysis: high MFI value corresponds to low viscosity and molecular weight.

The apparatus (Figure 22) is described in ASTM D 1238 – 04 [69] and is composed of a hollow cylinder that act as heat supplier through

- A vertical hollow cylinder that act as heating system with maximum deviation of  $\pm 1^\circ\text{C}$ . It is generally made of steel, even though, any material resistant to wear and corrosion under employed temperatures may be applied.
- A die and a piston fabricated with the same material of the cylinder.
- A set of removable weights. The maximum tolerance for piston and loads weight is 0.5%.
- A blade coupled with a timer in order to cut the melt polymer after passing through the die at fixed times ( $t_{cut-off}$ ).
- External balance with an accuracy of 0.1 mg

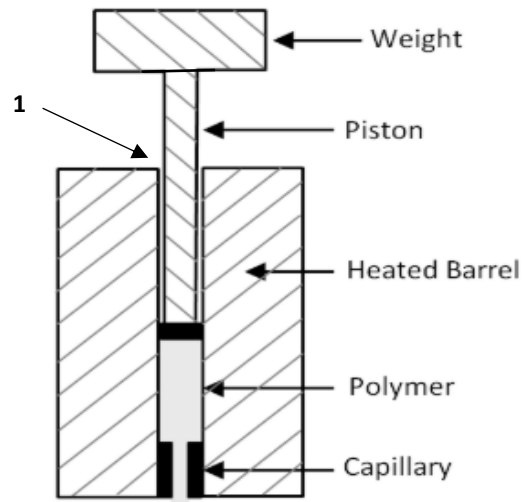


Figure 22. Representation of main component of melt flow indexer.

The test specimens are introduced in any form, such as pellets, strips of film and molded slugs at the top of the hole of the cylinder (Point 1 in Figure 22). In case of particular material (e.g. polymers containing volatile components or highly reactive) it is compulsory to pre-treat samples, for example, by conditioning them in a dryer.

For what concerns the experimental procedure, it is explained, equivalently, by ISO 1133 [68] and ASTM D 1238-04 [69] and can be summarized in the following steps:

The main factors can lead to a decrease of this technique precision are thermal degradation or cross-linking phenomena and filler morphology in composite materials.

The tests were performed on PS samples as supplied, without any pre-treatment by mean of an “InstronCeast MF20”. The mass was applied 240s after filling the MFI cylinder with  $5 \pm 0.2$  g of material; data acquisition started 30 s later; cut samples were weighted after 20 minutes from end of test. Testing temperatures and testing masses were 180°C/ 5kg for polystyrenes and 190°C/ 21.6kg for HDPE. Cut times ( $t_{\text{cut-off}}$ ) were 25 s, 250s and 15s for PS 2982, PS2380 and HDPE, respectively

### 2.3.2. Determination of intrinsic viscosity

Intrinsic viscosity ( $[\eta]$ ), also known as limiting viscosity number, is an index that describe the effect of solute on viscosity of a solution. It is evaluated by following ASTM D2857-16 [71] (or ISO 1628 [72]) and ISO 3105 [73] and is defined as:

$$[\eta] = \lim_{c \rightarrow 0} \left( \frac{\eta - \eta_0}{c \eta_0} \right) \quad (\text{Eq. 36})$$

Where  $\eta$  is the solution viscosity,  $\eta_0$  is the pure solvent viscosity and  $c$  is the polymer concentration in the solution.

The estimation of such a parameter allows to determine quantitatively the molecular weight of a polymer, dissolved in a proper solvent, by mean of Mark-Houwink equation:

$$[\eta] = K (M_w)^a \quad (\text{Eq. 37})$$

Where  $M_w$  is the polymer molecular weight, while  $K$  and  $a$  are two tabulated constants depending on polymer-solvent system and on temperature. In particular, for what concerns solvents, a value  $a=0.5$  indicates a theta solvent (i.e. limiting condition for good solvents), while a value  $a=0.8$  is typical of good solvents. Throughout this work molecular weight of both polystyrene N2982 and N 2380 has been evaluated by using toluene solvent, i.e.  $K= 0.012 \text{ cm}^3/\text{g}$ ,  $a=0.714$  and  $T=30^\circ\text{C}$  [70].

As for the standards, viscosity values (i.e.  $\eta$  and  $\eta_0$ ) are determined by measuring flow time of a solution through a capillary, considering that higher flow times corresponds to higher viscosity value.

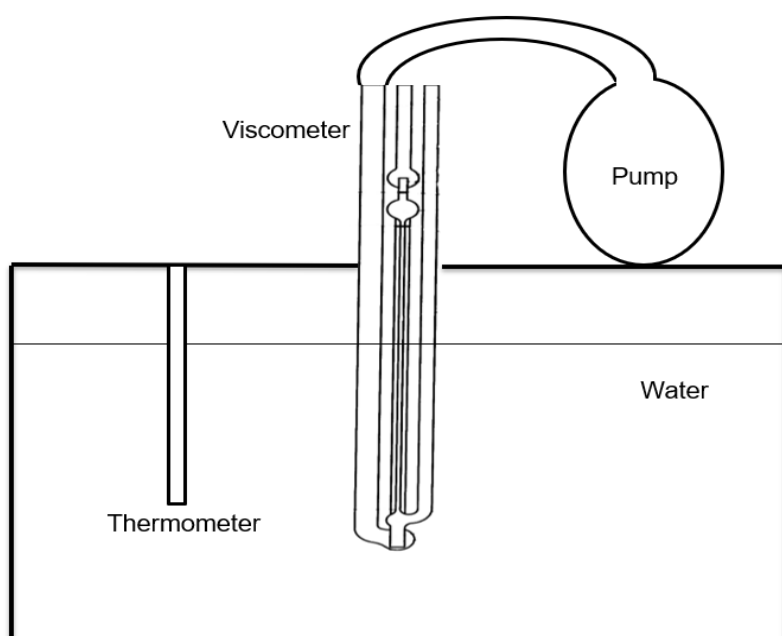


Figure 23 (above). Schematic representation of capillary viscometer apparatus

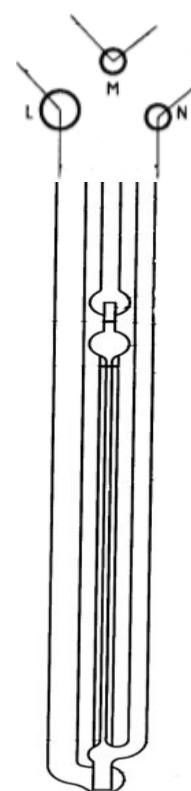


Figure 24 (right). Representation of a BS/IP/MSL viscometer [73]

The apparatus (Figure 23) is composed of a thermostatic bath (i.e. water) with an accuracy of  $\pm 0.01^\circ\text{C}$ , a pumping system, an external timer with an accuracy of  $\pm 0.1 \text{ s}$  and a capillary viscometer made of low expansion, fully annealed borosilicate glass [73]. In this work was used a BS/IP/MSL viscometer (Figure 24) and a manual pump.

A diluted type solution has been used in order to assure homogeneity and, therefore, has been performed through two steps. The first consist of preparation of a concentrated solution (i.e. 20 mg/ml), which is then properly diluted in order to obtain the desired concentrations. In this

project a concentrated solution of C=20 mg/ml (5 g of PS dissolved in 250 ml of toluene) has been diluted to obtain 5 ml sample solutions of 4 mg/ml, 8 mg/ml, 12 mg/ml and 16 mg/ml.

Due to the high sensitivity of the apparatus, measurement repeatability has to be checked i.e. a reliable flow time is obtained from a set of minimum three tests. A test is considered reliable only if the difference between two subsequent observed times is lower than 0.25%.

Once the efflux time for pure solvent and solution has been estimated, it is possible to estimate solvent and solution viscosities by mean of the following equation:

$$\eta = Ctp - E \frac{\rho}{t^2} \quad (\text{Eq. 38})$$

Where:

- $\eta$  is the estimated viscosity
- C and E are constants depending to the viscometer type and dimensions. For the considered one C=0.001, while the value of E has not been provided due to the negligibility of the second term of the equation for high flux times ( $t > 200s$ )
- $\rho$  is the sample density
- t is the efflux time

At this point it is possible to calculate, equivalently, logarithmic viscosity number (also known as inherent viscosity) or reduced viscosity (RV) as:

$$LVN = \frac{\ln(\eta/\eta_s)}{c} \quad (\text{Eq. 39})$$

$$RV = \frac{\eta - \eta_s}{c \eta_s} \quad (\text{Eq. 40})$$

Where  $\eta$  and  $\eta_s$  are, respectively, solution and solvent viscosity and c is the polymer concentration within the considered solution.

By plotting the obtained LVN (or RV) values for solution at different concentration as a function of concentration itself, a linear regression is performed. Intrinsic viscosity is estimated as the intercept of this line with the zero- concentration axis (figure 25). Moreover, in order to provide an evaluation of measurement accuracy, it is possible to relate the  $[\eta]$  values estimated by mean of reduced viscosity and logarithmic viscosity number: small difference indicates high measurement reliability.

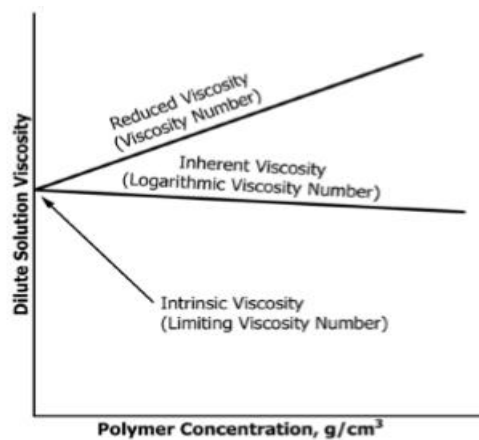


Figure 25. Example of plot used to estimate intrinsic viscosity [71]

## 2.4. Thermo-mechanical degradation

Mechanical stress has been applied to melt polymer by mean of a Brabender measuring mixer, which is a machine for non-continuous production of well dispersed polymeric, elastomeric and ceramic mixtures.

The apparatus, made of stainless steel, is composed of a mixing chamber (Figure 26) with two counter-rotating blades, a quick loading chute, a heating and temperature control system with an accuracy of  $\pm 0.5$  °C and a drive unit (i.e. torque rheometer) to record temperature, torque (T) and rotation velocities of blades ( $v_1 = 1.5v_2$ ) during the processing.

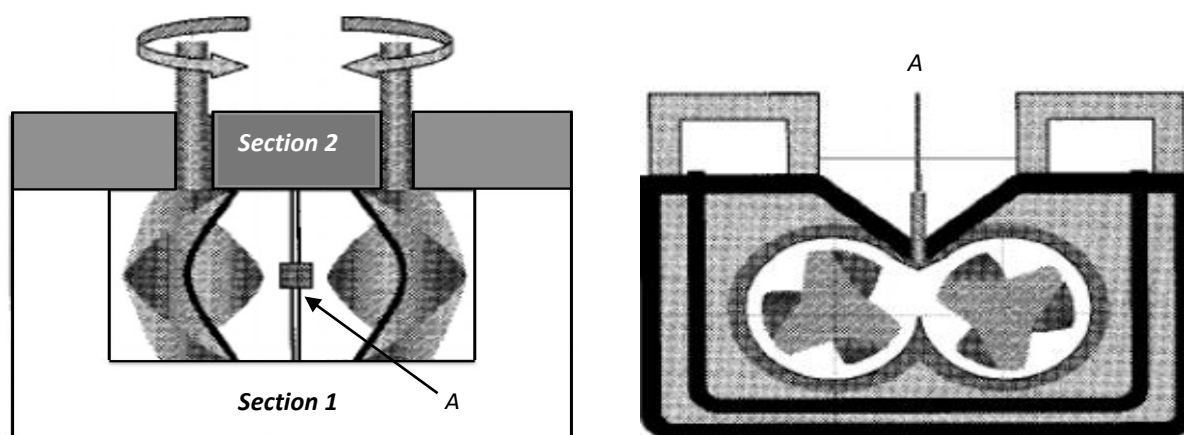


Figure 26. Schematic representation of Brabender mixer chamber: above (left) and front view (right) [84]

The last two parameters allow to estimate the mechanical energy provided to the specimen and, therefore, allow a processability assessment.

The chamber is composed of two detachable zones (section 1 and 2 in Figure 26), each with an independent heating and temperature control system.

Mixing blades exist in many different geometries according to the required application fields, i.e. sample material and volume. During tests performed in this project, a series W 50 EHT mixer equipped with a roller-type blade was used. The extension EHT (electric, high temperature) indicates an electric heating system coupled with a compressed air cooling system. This configuration is particularly suited for study of thermoplastic polymers with high melting temperature as it allows a maximum temperature of 500°C.

The samples to be mixed have to be prepared in form of powder or pellets, so that torque value remains below the maximum value allowed by the apparatus, i.e. 100 Nm for the employed mixer. Introduced sample quantity varies according to the used chamber and should be enough to fill 80% of its volume.

Blade type	Application example	Compatible mixer series
Roller (W)	Thermoplastics	15, 30, 50 and 350
Cam (N)	Elastomers, caoutchouc	50 and 350
Branbury (B)	Elastomers, caoutchouc	50 and 350
Sigma (S)	PVC dry blends	50, 300 and 350
Delta (MB)	Thermosetting polymers	30 and 50

Table 5. Application field for different mixing blades.

Test parameters and mixer type has to be selected within characteristic tabulated ranges for the studied material. For what concerns polystyrene, the standard suggests a range of 180-200°C for temperature and 30-60 rpm for blade rotation speed.

Moving on to the procedure, it is described by ASTM 2538 [74] and can be summarized as follow:

- Heat both sections at the desired temperature and check the cleanness degree of the apparatus. Cleaning process has to be performed with tools and/or solvents that does not affect the chamber, e.g. brass tools and/or toluene. This step is crucial for results reliability.
- Select and operate blades rotation speed and insert the sample from above (Point A in figure 24). Then seal the chamber and, simultaneously, initiate the torque recording device. The sample has to be introduced all at once in order to obtain a homogeneous melting and, therefore, a more accurate result.
- The test conclusion is differently determined according to the test objective. In this work analysis terminated at a time (t) corresponding to a predetermined value of absorbed energy (i.e. ).  
Other possibilities include achievement of a steady state by torque (fusion test), sudden rise of torque due to degradation initiation (thermal stability test) and achievement of a certain color shade due to degradation (color-hold stability test).
- Open the chamber by separating sections 1 and 2, collect the sample in a proper storage and clean the device using the above mentioned tools.

The typical plot from mixing (Figure 27) can be exploited to analyze material behavior.

Material initial grinding is described by the A-B region ( $t_{A-B} \approx 1$  min), where the initial peak ( $T_{load}$ ) corresponds to the loading of initial cold raw material, which is then grinded while still glassy.  $T_{load}$  and  $t_{A-B}$  depend on particle size, so,

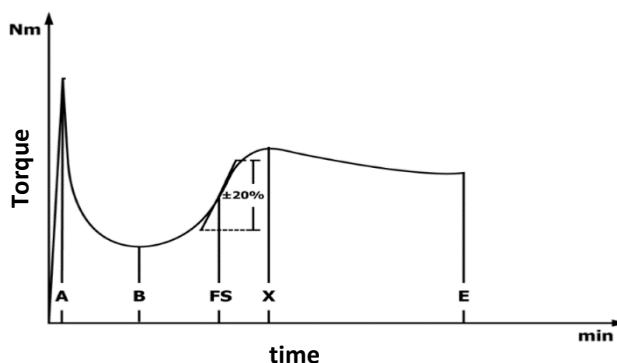


Figure 27. Typical torque rheometer fusion test curve [84]

for analysis of high modulus materials, the use of powder samples is preferred to pellet ones.

Melting process (section B-X) takes place once material overcomes its melting temperature (for semicrystalline polymers) or glass transition temperature,  $T_g$ , (for amorphous polymers) and, consequently, a high viscosity fluid form. The recorded torque value increases until it reaches a maximum value ( $T_{max}$ ) corresponding to the chain breaking point. From point B, indeed, polymeric chains are stretched by the mechanical input until chain scission initiate (point X).

Moreover, derivative at the inflection point (FS) can be exploited to roughly estimate melting speed:

$$Melting\ speed = \frac{dT(FS)}{dt} \pm 20\% \quad (\text{Eq. 41})$$

In section X-E it can be observed a torque decrease due to rupture of polymeric chains. Mechanical stress initiate degradation process at point X, leading to a decrease in recorded torque until point E where shear stress degradation becomes negligible.

Material behavior after point E depends on its properties, i.e. material may undergo further degradation by means of other phenomena (heat, oxidation) activated by applied mechanical stresses [84].

## 2.5. Applicability of Ozawa-Flynn-Wall method

A verification of thermal endurance data estimated by mean of Ozawa-Flynn-Wall method has been performed by subjecting samples of different mass to a constant temperature and measuring the mass variation.

The test has been carried out in a ventilated oven at 200°C, 220°C and 250°C for 90, 180, 200, 220, 270 and 360 minutes and, afterwards, the samples have been weighted by mean of a high accuracy balance with an error of  $\pm 0.3$  mg.

Used samples were characterized by different mass and different ratio between environment exposed area and volume:

- S1: 20 mg in a Petri dish with a diameter of 50 mm ( $A/V=1.74$  mm<sup>-1</sup>)
- S2: 2 g in a refractory crucible ( $A/V=0.35$  mm<sup>-1</sup>)
- S3: 10 g in an aluminum cup 60 mm ( $A/V=0.24$  mm<sup>-1</sup>)
- S4: 10 g a Petri dish with a diameter of 100 mm ( $A/V= 0.55$  mm<sup>-1</sup>)



## 3. Experimental results

### 3.1. Thermogravimetric Analysis

The main information obtainable from the above defined programs is the degradation curve, which can lead to the estimation of other parameters such as the activation energy plot and the thermal endurance curves.

The collected results will be presented, starting from high density polystyrene (HDPE) .

#### 3.1.1. High density polyethylene

Literature [77] reports for HDPE a rather simple degradation path. For this reason, it was investigated in order to set up the measurement and analysis procedure and check its validity.

TGA and DTG plots (Figure 28) show a single step reaction, with a first order kinetic. As can be noticed high heating rates shift TG curve toward higher temperatures. The obtained results were comparable to the ones obtained by Alonso et al. [93] (Figure 29), confirming the validity of the employed method.

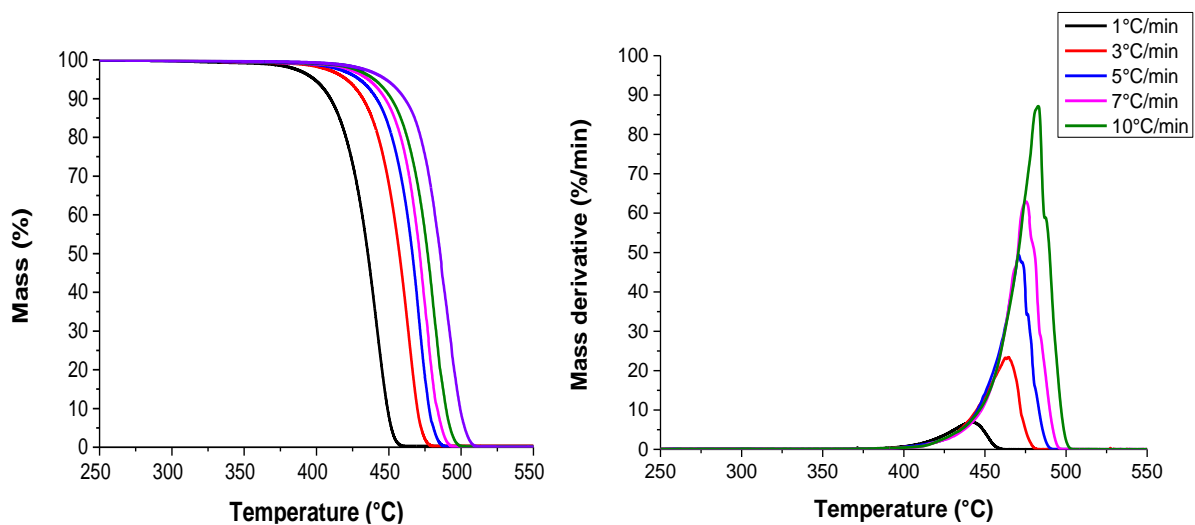


Figure 28. Standard TGA (left) and DTG (right) of HDPE performed at 1°C/min, 2°C/min, 3°C/min, 5°C/min, 7°C/min, 10°C/min in nitrogen atmosphere.

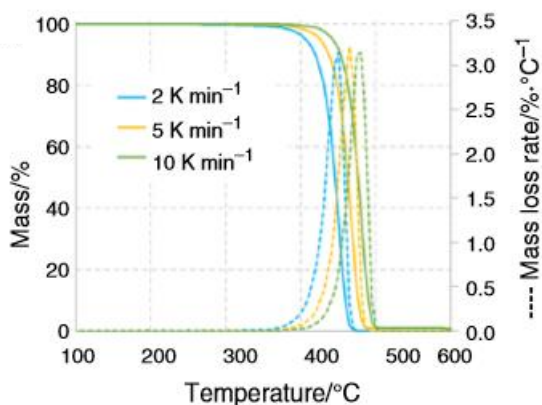


Figure 29. Standard TGA (continuous line) and DTG (dotted line) of HDPE [93]

### 3.1.2. Polystyrene N2982 (low $M_w$ )

Thermogravimetric analyses performed in nitrogen atmosphere at different heating rate led to the degradation curves plotted in Figure 30. As can be noticed from the smooth shape and from the single peak of DTG, the degradative process is characterized by a single reaction, which can be identified as random scission reaction. Therefore, as confirmed from Equation 25 and data found in literature [76], a first order kinetics can be assumed for the entire system:

$$n = \frac{d \ln \left( \frac{dC}{dt} \right)}{d \ln(1 - C)} = 1.083 \quad (\text{Eq. 42})$$

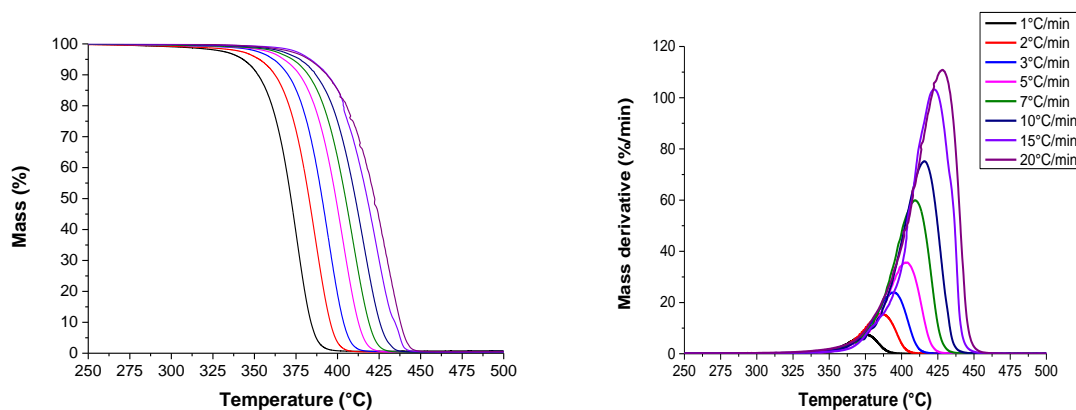


Figure 30. Standard TGA (left) and DTG (right) of polystyrene N2982 performed at 1°C/min, 2°C/min, 3°C/min, 5°C/min, 7°C/min, 10°C/min, 15°C/min and 20°C/min in nitrogen atmosphere.

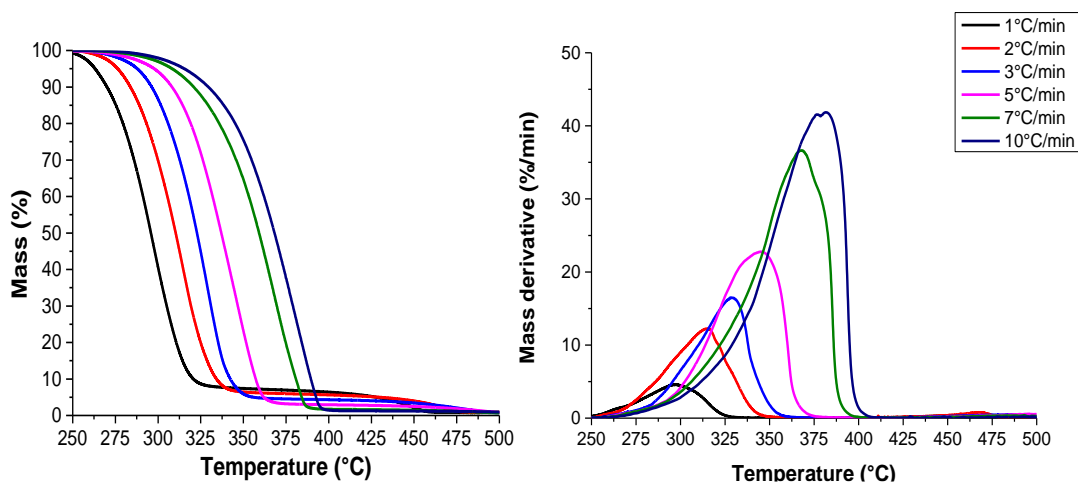


Figure 31. Standard TGA (right) and DTG (left) of polystyrene N2982 performed at 1°C/min, 2°C/min, 3°C/min, 5°C/min, 7°C/min, 10°C/min in oxygen atmosphere.

It can be noticed that degradation initiation temperature ( $T_{init}$ ) is strongly dependent on heating rate (HR), ranging between a value of 320°C for HR=1°C/min up to 385°C for HR=20°C/min. A residue of  $\approx 1.5\%$  wt. has been observed in all PS tests, probably due to presence of some additives; indeed, polystyrene thermal-degradation process leads to complete degradation [76].

The resulting curves from thermogravimetry in air (Figure 31) shows a lower  $T_{init}$  with respect to the ones performed in pure nitrogen and a kinetic order  $n=1.45$ . This behavior can be explained by the different reaction pathways for PS thermal and thermo-oxidative degradation. Indeed, back-biting reaction (oxidation) immediately affect sample weight, while chain scission reaction (thermal) statistically requires a higher time in order to cause mass loss.

The plateau (secondary peak in DTG) observed at low heating rates (HR<5°C/min) at T=325-450°C corresponds to a high activation energy ( $E_a$ ) phase, which, according to literature [77], can be attributed to degradation process of intermediate compounds produced during oxidation.

### 3.1.3. Polystyrene N2380 (high $M_w$ )

Thermogravimetric analysis performed in nitrogen (Figure 32) did not evidence any difference in the behavior of the two polystyrenes, besides a small variation at high heating rates (Figure 34), which suggest a slight degradation resistance increase for high molecular weight PS. The estimated reaction order is  $n=1.11$ .

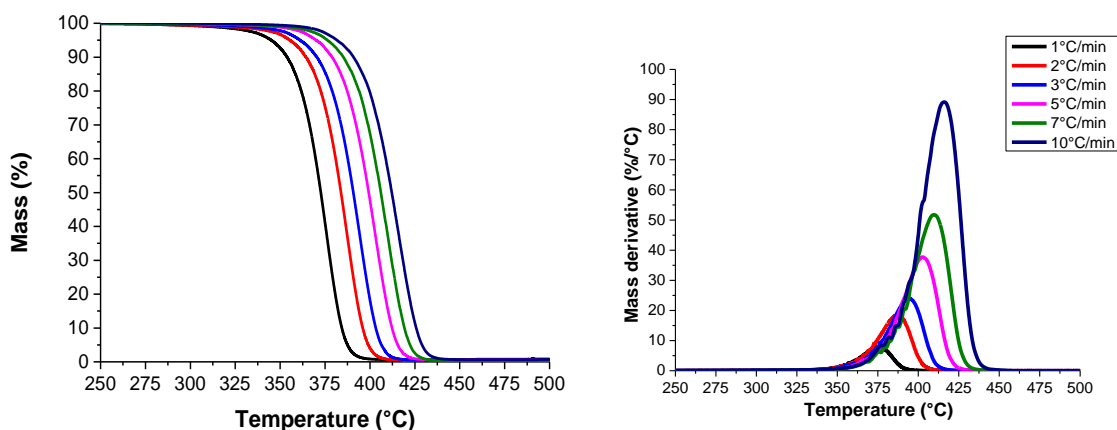


Figure 32. Standard TGA (left) and DTG (right) of polystyrene N2380 performed at 1°C/min, 2°C/min, 3°C/min, 5°C/min, 7°C/min, 10°C/min, 15°C/min and 20°C/min in nitrogen atmosphere.

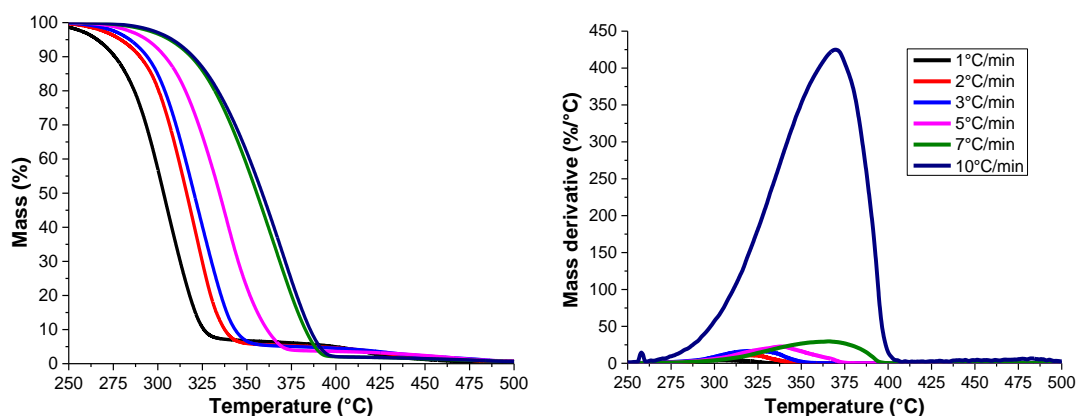


Figure 33. Standard TGA (right) and DTG (left) of polystyrene N2380 performed at 1°C/min, 2°C/min, 3°C/min, 5°C/min, 7°C/min, 10°C/min in oxygen atmosphere.

This suggest a slight property increase for high molecular weight PS. The estimated reaction order is  $n=1.11$ .

The resulting curves from TGA in air environment (Figure 33) show a considerable behavior variation for different molecular weight and heating rate. As matter of facts, at low heating rates ( $HR < 5^\circ\text{C}/\text{min}$ ) PS N2380 shows a better degradation resistance, although, the intermediate phase is characterized by a lower stability. At high heating rates ( $HR > 7^\circ\text{C}/\text{min}$ ), instead, low molecular weight PS shows higher degradation resistance.

The estimated reaction order is  $n=1.36$ .

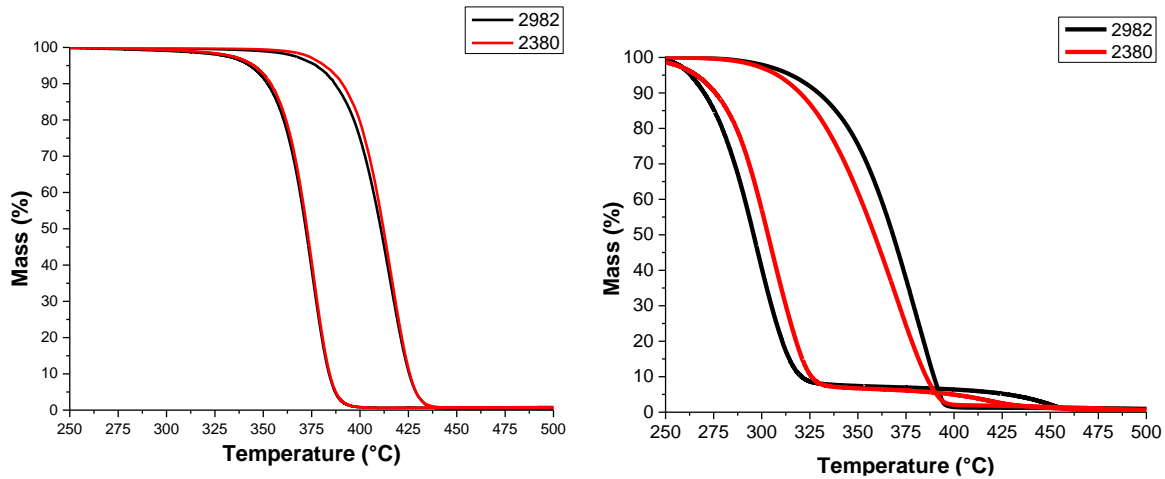


Figure 34. Comparison of TGA of PS N2982 (black) and PS N2380 (red) at  $1^\circ\text{C}/\text{min}$  and  $10^\circ\text{C}/\text{min}$  performed in nitrogen (left) and air (right)

### 3.2. Melt flow index

Polystyrene MFI test were initially performed at 200°C, as suggested by literature, and the outcome is represented in Figure 35, where each line represent a test.

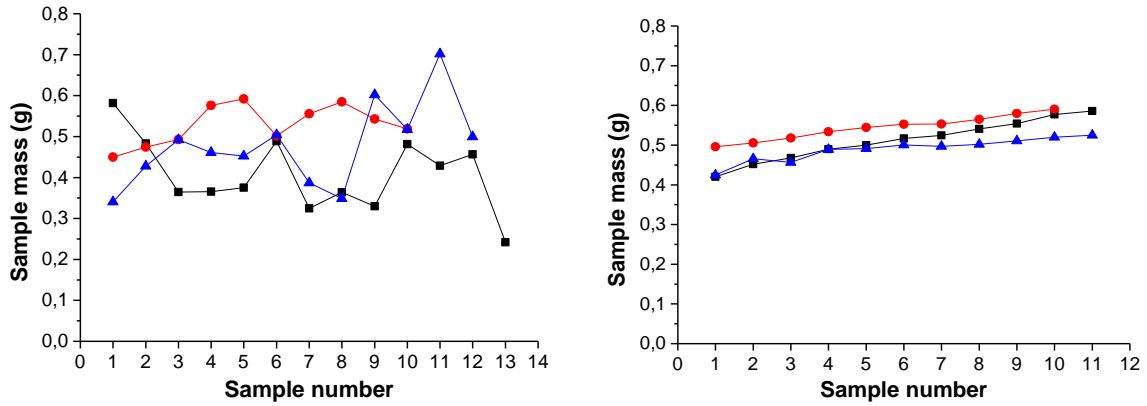


Figure 35. Cut thread masses resulting from MFI test (200°C, 5kg) for PS N2982 (left) and PS N2380 (right)

As can be noticed, results obtained for PS N2982 (left) were characterized by low repeatability and wide spacing. This feature has been probably caused by the high fluidity of PS N2982 and the device lack of cutting precision. The estimated melt flow indexes for the two polystyrenes were:

$$MFI_{2982}(200^{\circ}\text{C}, 5\text{kg}) = \frac{600 m_{av}}{t_{cut-off}} = 21.9 \pm 4.24 \frac{\text{g}}{10 \text{ min}} \quad (\text{Eq. 43})$$

$$MFI_{2380}(200^{\circ}\text{C}, 5\text{kg}) = \frac{600 m_{av}}{t_{cut-off}} = 2.06 \pm 0.24 \frac{\text{g}}{10 \text{ min}} \quad (\text{Eq. 44})$$

Due to the results high error, test has been repeated at temperature of 180°C in order to limit PS flow. Resulting data are described in Figure 36.

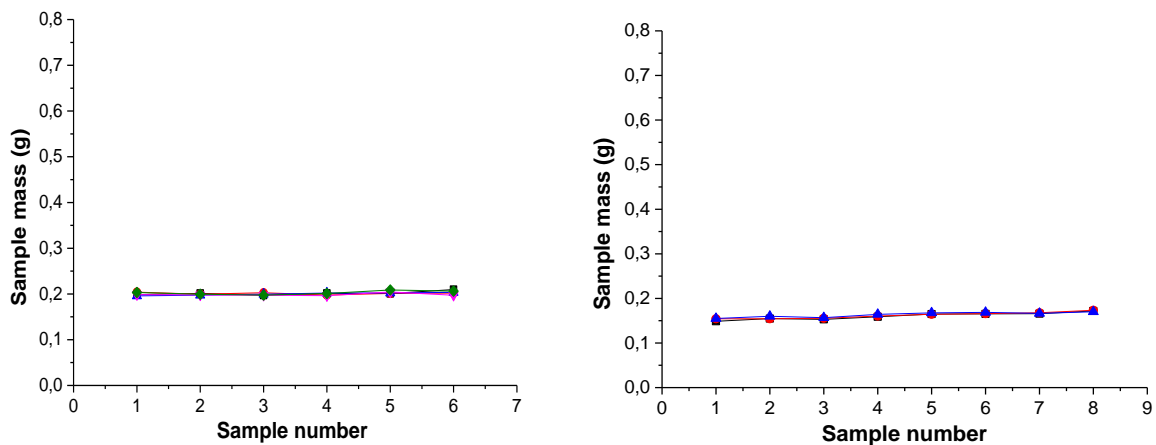


Figure 36. Cut thread masses resulting from MFI test (180°C/ 5kg) for PS N2982 (left) and PS N2380 (right)

The new outcome highlights much stable results and, therefore, a much more accurate MFI estimation can be provided:

$$MFI_{2982}(180^{\circ}C, 5kg) = \frac{600 m_{av}}{t_{cut-off}} = 4.82 \pm 0.11 \frac{g}{10 min} \quad (\text{Eq. 45})$$

$$MFI_{2380}(180^{\circ}C, 5kg) = \frac{600 m_{av}}{t_{cut-off}} = 0.398 \pm 0.023 \frac{g}{10 min} \quad (\text{Eq. 46})$$

Moreover, MFI test has been performed on PS N2982 after being subjected to mechanical shear stress (i.e. Brabender mixer) for a total applied energy E= 400 kJ. The resulting data (Figure 37) showed, as expected, an increase in MFI value due to reduction in molecular weight caused by degradation process.

$$MFI_{2982}^I(180^{\circ}C, 5kg) = \frac{600 m_{av}}{t_{cut-off}} = 16.345 \pm 0.318 \frac{g}{10 min} \quad (\text{Eq. 47})$$

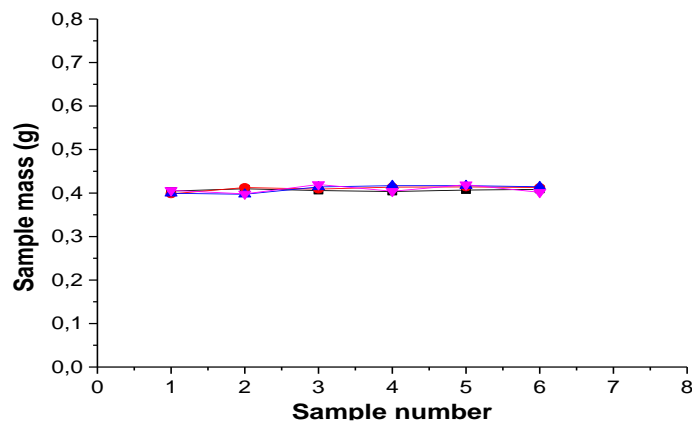


Figure 37. Cut thread masses resulting from MFI test (180°C/ 5kg) for PS N2982

For what concerns HDPE, tests at 190°C led to the following results (Figure 38).

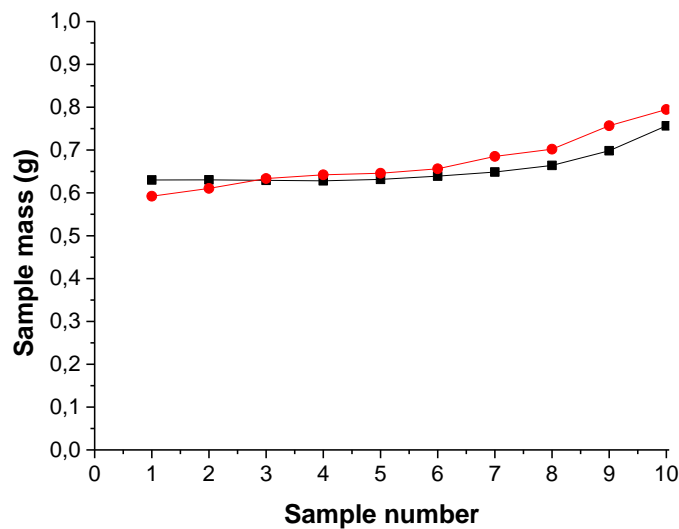


Figure 38. Cut thread masses resulting from MFI test (190°C/ 21.6 kg) for HDPE

The resulting MFI has been estimated with high accuracy as:

$$MFI_{PC}(300^{\circ}C, 1.2 \text{ kg}) = \frac{600 m_{av}}{t_{cut-off}} = 26.55 \pm 3.29 \frac{g}{10 \text{ min}} \quad (\text{Eq. 48})$$

Finally, melt flow indexes obtained in these tests showed a good agreement with data found in literature:  $MFI_{2982}(200^{\circ}C, 5 \text{ kg}) = 25 \text{ g}/10\text{min}$  [94],  $MFI_{2380}(200^{\circ}C, 5 \text{ kg}) = 2 \text{ g}/10\text{min}$  [95] and  $MFI_{PC}(300^{\circ}C, 1.2 \text{ kg}) = 26.2 \text{ g}/10\text{min}$  [96].

### 3.3. Viscometer

Figure 39 represents the obtained logarithmic viscosity number (or reduced viscosity) and the linear regression performed to estimate intrinsic viscosity of PS N2982 (left) and PS N2380 (right).

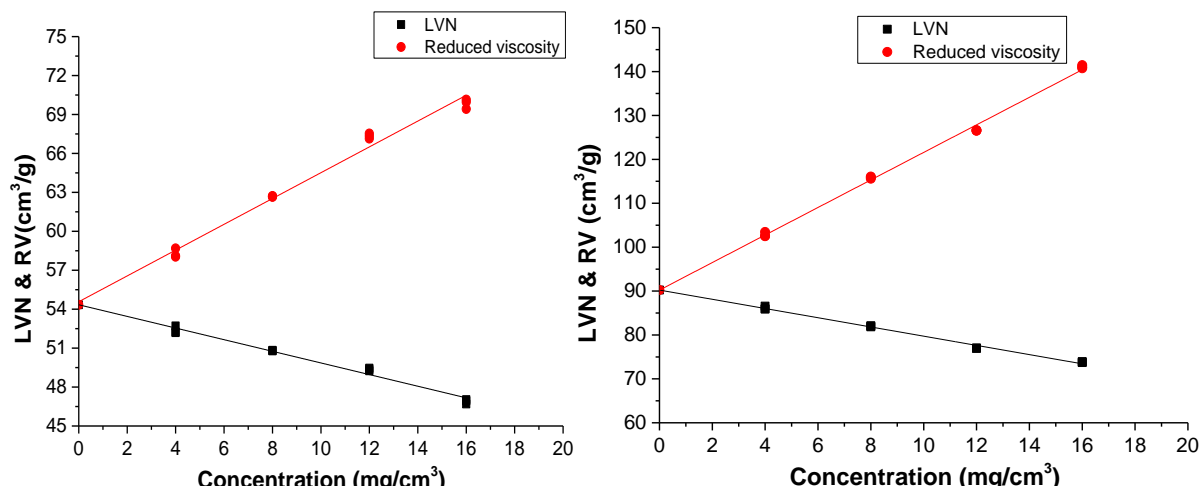


Figure 39. Experimental plot to determine intrinsic viscosity of PS N2982 (left) and PS N2380 (right)

The evaluated intrinsic viscosity have been found to be  $[\eta]_{N2982} = 54.339 \pm 0.177 \text{ cm}^3/\text{g}$  and  $[\eta]_{N2380} = 90.22688 \pm 0.273 \text{ cm}^3/\text{g}$ , which correspond, respectively, to a molecular weight  $MW_{N2982} = 131931 \pm 1382 \text{ g/mol}$  and  $MW_{N2380} = 268403 \pm 374 \text{ g/mol}$ .

This result confirm the qualitative analysis operated by MFI test, i.e. PS N2982 presents a lower molecular weight with respect to PS N2380.

Molar mass values have been compared with the ones obtained by GPC test (externally provided), for whom a comparison is provided in Table 6.

	Experimental	Literature	Error
<b>PS N2982</b>	131931	124016	6%
<b>PS N2380</b>	268403	274595	2%

Table 6. Comparison between data obtained with above explained method and by GPC (Versalis)

The accuracy variation with molecular weight may be due to the lack of measuring precision for small efflux time, hence, low MW polymers generally presents a higher error.

Furthermore, as for MFI analysis, viscometry test has been performed on PS N2982 after being subjected to the above mentioned mechanical shear stress (figure 39).

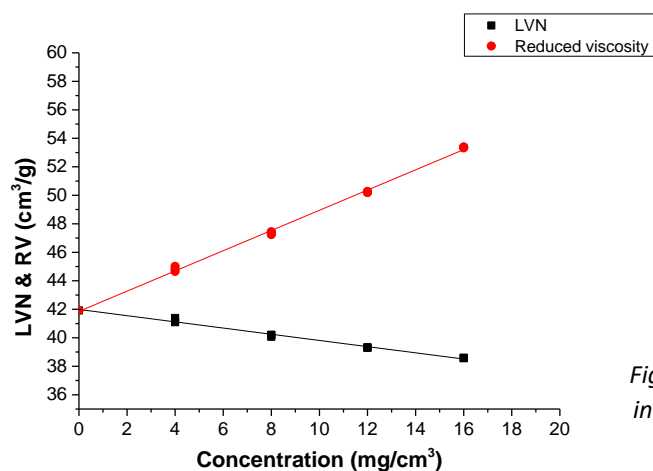


Figure 40. Experimental plot to determine intrinsic viscosity of PS N2982 after being subjected to mechanical stress

As can be noticed, LVN and reduced viscosity linear regressions intersect at the intrinsic viscosity value, which is  $[\eta]^{MS}_{N2982} = 41.9206 \pm 0.5477 \text{ cm}^3/\text{g}$ . The estimated molecular weight (i.e.  $MW^{MS}_{N2982} = 91734 \pm 1989 \text{ g/mol}$ ) show a consistent average chain length reduction due to the applied mechanical stress.



## 4. Analysis and discussion

### 4.1. Thermogravimetric Analysis

#### 4.1.1. Polystyrene 2982

The estimated order of reactions ( $n_{\text{air}}= 1.45$ ,  $n_{\text{nitrogen}}= 1.083$ ) allow the application of OFW method for estimation of thermal endurance curves, which have been calculated for constant conversion percentage ( $\alpha$ ): 2%, 5%, 10%, 30%, 40%, 50% and 75%.

Firstly, failure temperatures ( $T_f$ ) have been obtained from TGA plot for different heating rate programs ( $\beta \leq 10^\circ\text{C}/\text{min}$ ) and fixed failure criteria ( $\alpha$ ). The determined values, then, have been plotted as function of heating rate logarithm and a linear regression have been performed (Figure 41)

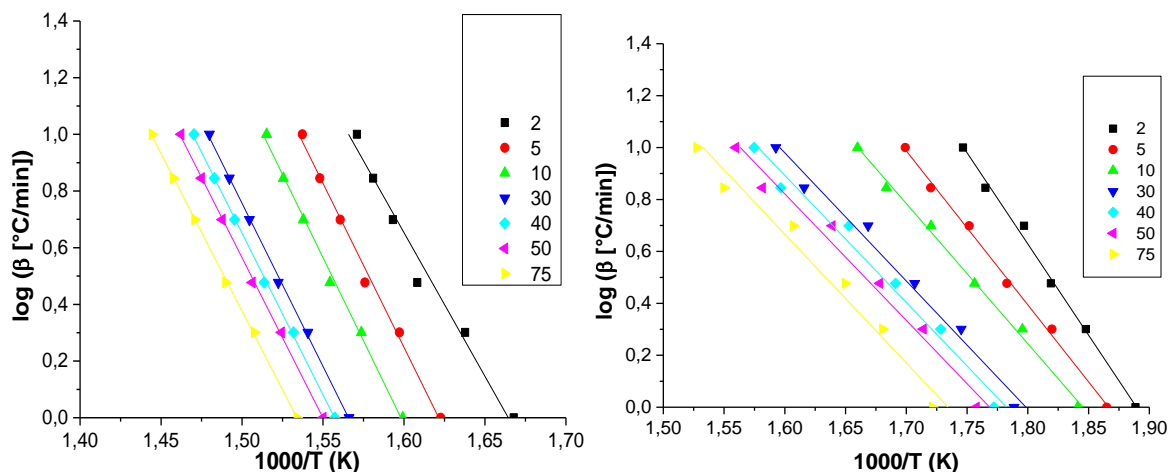


Figure 41. Plot of heating rate as function of temperature reciprocal in nitrogen (left) and air (right) for  $\alpha= 2\%$ , 5%, 10%, 30%, 40%, 50% and 75%, ordered from right to left.

Linear regression slope and error have been exploited for a first estimation of activation energy by mean of Equation 11, which have then been corrected by mean of Doyle's correction factor (b). The estimated activation energies have been plotted in figure 42 with the relative error bars.

After an initial irregular transition domain, activation energy value reaches a region where it firstly slightly decrease and formerly ( $\alpha > 60\%$ ) stabilizes to values of 201 kJ/mol and 81 kJ/mol for degradation in nitrogen and air respectively.

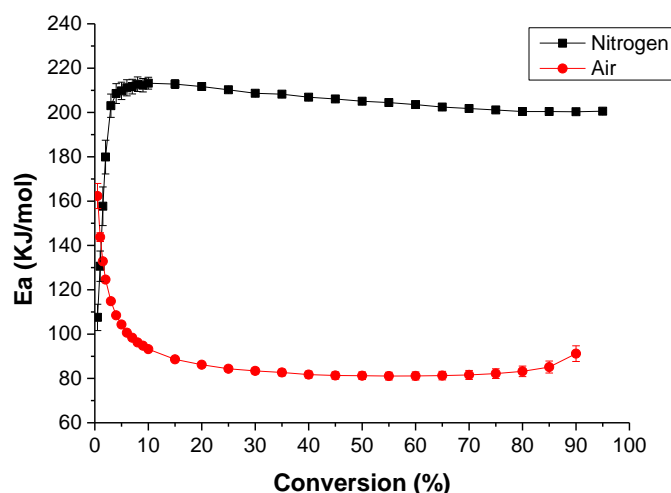


Figure 42. Plot of activation energies obtained with OFW method as function of mass loss percentage in nitrogen (black) and air (red).

As expected from literature, PS thermal degradation presents an initial degradation ( $\alpha < 10\%$ ) characterized by rupture of weak bonds, i.e. random distributed defects. Subsequently, the observed plateau at high  $E_a$  values indicates the occurrence of degradation of defect-free chains. The slight activation energy decrease throughout the process will be commented later. For what concerns behavior in air atmosphere, the opposite trend can be explained by reminding that propagation reaction of oxidative process (i.e. back-biting) is characterized by higher kinetic with respect to pure thermal degradation one, feature that can explain the lower activation energy.

<b>a =</b>	<b>2%</b>	<b>5%</b>	<b>10%</b>	<b>30%</b>	<b>40%</b>	<b>50%</b>	<b>75%</b>
<b>T<sub>f</sub> (N<sub>2</sub>)=</b>	354.52°C	367.60°C	377.10°C	391.48°C	395.56°C	398.98°C	406.76°C
<b>T<sub>f</sub> (air)=</b>	283.38°C	297.70°C	308.12°C	326.18°C	331.87°C	336.99°C	349.11°C

Table 7. Failure temperatures ( $\beta=5^\circ\text{C}/\text{min}$ ) of PS 2982 in nitrogen and air environment for constant conversion values of 2%, 5%, 10%, 30%, 40%, 50% and 75%.

The estimated  $E_a$  values and corresponding failure temperatures obtained for intermediate heating rate (i.e.  $5^\circ\text{C}/\text{min}$ ) (Table 7), have been exploited for computation of thermal endurance (TE) curves, by mean of Equation 32. The variable has been computed for a temperature range between 150 and  $450^\circ\text{C}$  in both nitrogen and air atmosphere and the obtained thermal endurance curves are shown in figure 43.

TE plots gives a different and more practical representation of above presented assessment. For heat induced degradation in nitrogen, an initial reaction delay ( $\alpha < 10\%$ ) can be observed from the increased spacing between curves, whereas at higher degradation percentages ( $\alpha > 10\%$ ) the reduction of failure time difference indicates a slight reaction acceleration, due to activation energy decrease. Moreover, temperature have different effect on degradation process: initiation reaction temperature is more effective on initiation reaction with respect to propagation one.

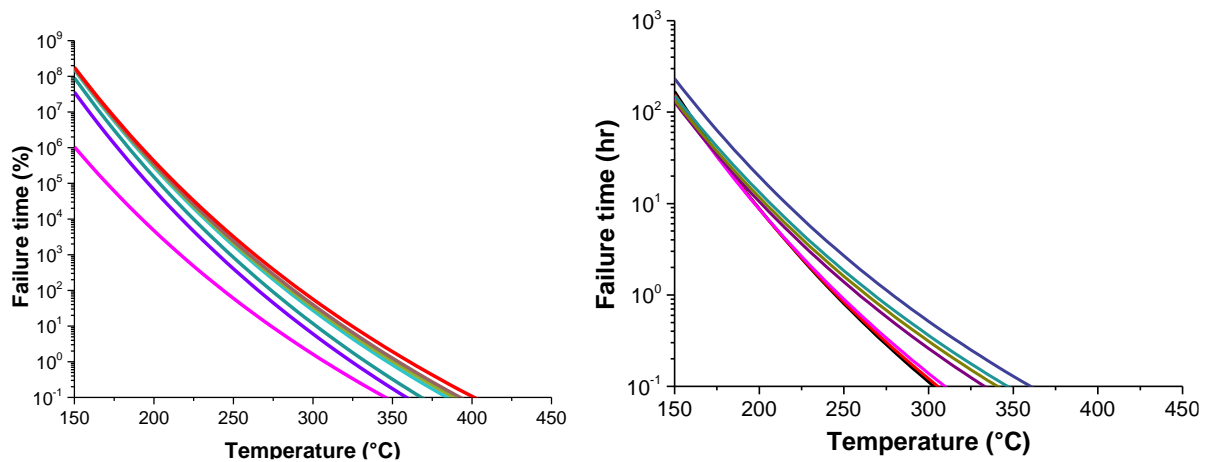


Figure 43. Thermal endurance curves of PS 2982 in nitrogen (left) and air environment (right) for conversion percentages of 2%, 5%, 10%, 30%, 40%, 50% and 75%, ordered from left to right

TE curves presented for test performed in air can be divided in three groups, corresponding to the three stages of PS thermo-oxidative degradation.

For low conversion values ( $\alpha < 10\%$ ), the proximity of TE curves pinpoints an acceleration in mass loss due to the transition from initiation (i.e. random chain scission) to propagation of reaction (i.e. backbiting). The central region ( $\alpha < 60\%$ ) is characterized by evenly spaced curves, which indicates a constant reaction rate for each temperature.

Finally, at high conversion ( $\alpha > 60\%$ ), a further reaction rate decrease have been registered, probably caused by the formation of a second phase characterized by higher heat resistance (i.e. activation energy).

The applicability of high heating rates ( $\beta > 10^\circ\text{C}/\text{min}$ ) on activation energy and thermal endurance curve estimation has been studied by performing the same calculation as above considering  $\beta$  values in a range between  $1^\circ\text{C}/\text{min}$  and  $20^\circ\text{C}/\text{min}$  (i.e. addition of  $15^\circ\text{C}/\text{min}$  and  $20^\circ\text{C}/\text{min}$  test with respect to above). The resulting failure temperatures have been plotted as function of  $\beta$  in order to estimate  $E_a$  values, which have been compared with the previously obtained ones (figure 45).

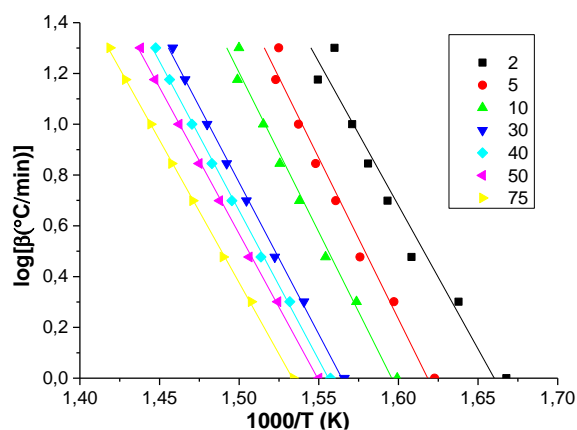


Figure 44. Plot of heating rate as function of reciprocal of temperatures obtained for heating rate range of  $1-20^\circ\text{C}/\text{min}$

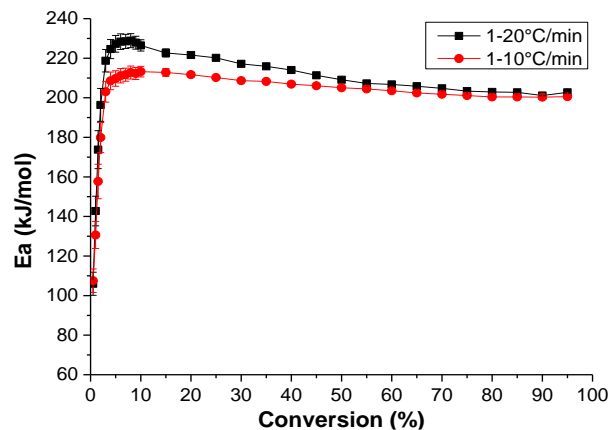


Figure 45. Plot of activation energies obtained for heating rate range of  $1-10^\circ\text{C}/\text{min}$  (red) and  $1-20^\circ\text{C}/\text{min}$  (black)

It has been noticed that the use of high heating rates leads to an overestimation of activation energy at low conversion rate. Indeed, as seen in figure 44,  $T_f$  values related with  $\beta=15^\circ\text{C}/\text{min}$   $\beta=20^\circ\text{C}/\text{min}$  present a strong divergence with respect to linear regression at conversion percentages up to  $\alpha =10\%$ . As consequence, failure times increase by a magnitude inversely proportional to conversion and applied temperature, as can be seen in figure 46.

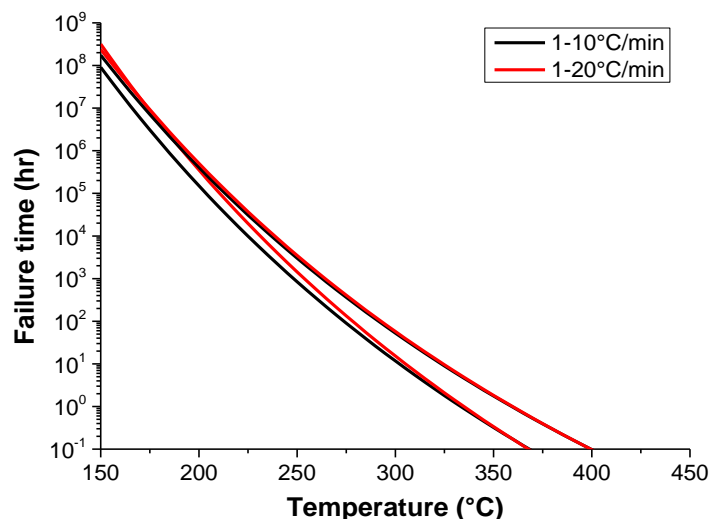


Figure 46. TE curves for conversion rates of 10% and 50% of PS 2982 obtained with activation energy obtained by employing TGA curves in range of 1-10°C/min (black) and 1-20°C/min (red)

In conclusion, a comparison between kinetic parameters obtained by mean of ISO 11358 [91] and ASTM 1641 [89] have been performed, although, no significative differences between the two methods have been observed.

#### 4.1.2. Polystyrene 2380

The effect of molecular weight has been evaluated by comparison of kinetic parameter obtained for PS N2982 ( $M_w=131931$  g/mol) and PS N2380 ( $M_w=268403$  g/mol).

Activation energy and TE plot have been computed for both nitrogen and air environment and the obtained graphs have been compared with the ones obtained for PS N2982 (figure 47 and 48).

Thermal degradation for high  $M_w$  (PS N2380) samples showed a more stable propagation reaction at conversion higher than  $C=10\%$  as can be seen from the flat  $E_a$  trend (i.e. 201 kJ/mol).

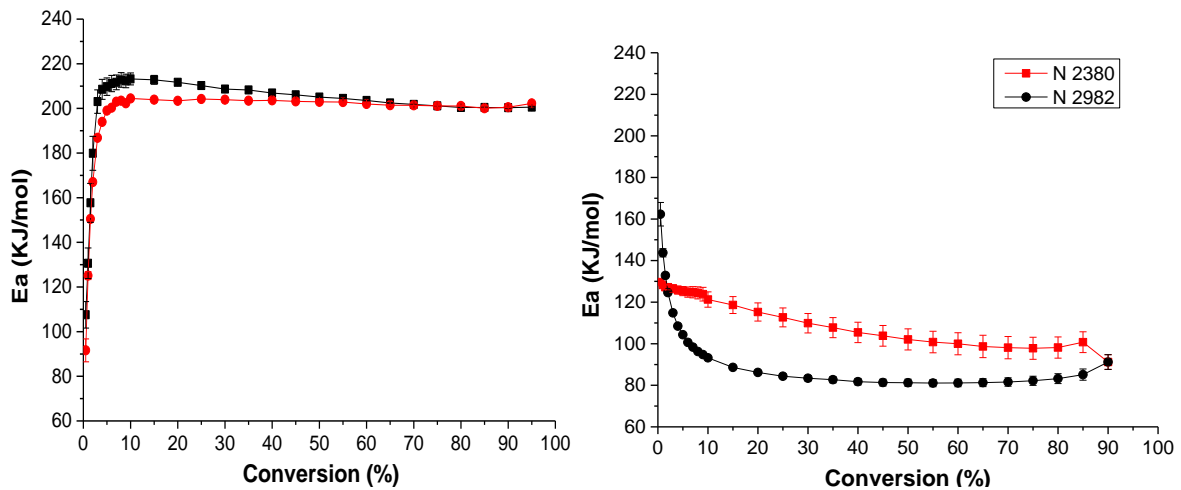


Figure 47. Plot of activation energies of PS N2982 (black) and PS N 2380 (red) in nitrogen (left) and air environment (right).

Moreover, the observed decrease in activation energy with respect to PS N2982 can be associated with the specific heat reduction for high molecular weight compounds. In particular, by considering the same thermal conductivity for the two samples,  $c_p$  ratio have been obtained by recording the internal temperature variation of high and low molecular weight polystyrenes subjected to a constant temperature of 250°C. The following expression was used:

$$\frac{c_p (N2380)}{c_p (N 2982)} = \frac{t (N2380) * m (N2982)}{t (N2380) * m (N2982)} = 0.94 \quad (\text{Eq. 49})$$

With  $t$ = time required to heat the sample up to 250°C and  $m$ = sample mass.

For what concerns degradation in air,  $E_a$  plot showed an opposite effect of molecular weight. As a matter of facts, activation energy (100-130 kJ/mol) increase with respect to PS 2982 depends on back-biting mechanism, whose reaction rate is proportional to molecular weight. As mentioned above, initiation process follow the same reaction path of heat-induced degradation, hence, activation energy at low conversion ( $\alpha < 2\%$ ) is lower for higher molecular weights.

Thermal endurance curve comparison for degradation in nitrogen and air environment is presented in figure 48 for  $\alpha=10\%$  and 50%.

Thermal degradation is characterized by a slight variation in failure time for  $\alpha < 35\%$ , while, at high conversion, an overlapping of TE curves of the two polystyrenes has been observed.

In conclusion, calculated TE for PS N2380 degradation in air environment highlighted a consistent increase in failure time. This effect remains substantially unchanged for  $\alpha$  values in the range of 5-95% and fades for isothermal conditions characterized by high temperature.

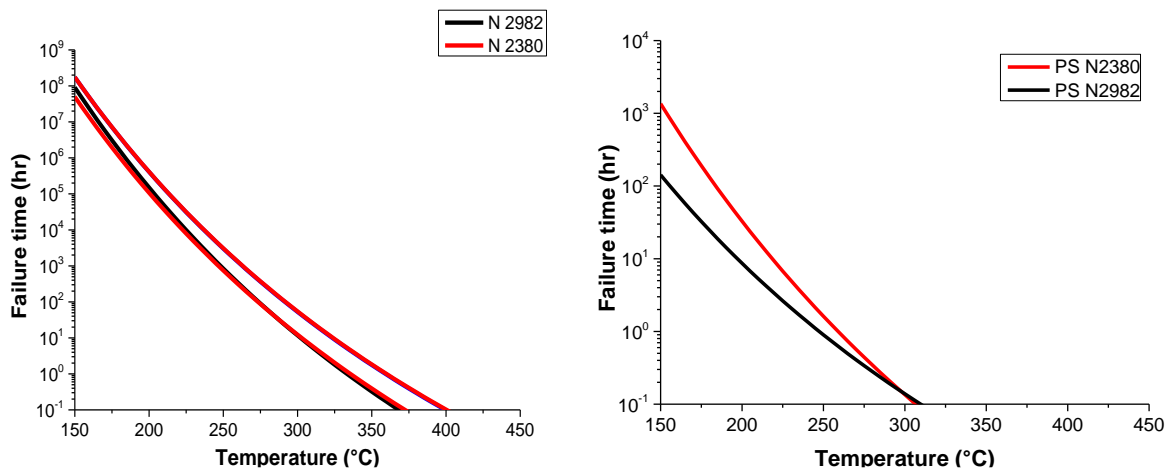


Figure 48. Thermal endurance curves of PS 2982 in nitrogen (left) and air environment (right) for conversion percentages of 10% and 50%.

### 4.1.3. High-density polyethylene

As for polystyrene, high-density polyethylene behavior in nitrogen atmosphere showed an initial ( $\alpha < 5\%$ ) sudden increase in activation energy (figure 49) due to weak bond breaking and volatilization of specimen different from HDPE (e.g. residual solvent). Then,  $E_a$  pass through a stable region ( $5\% < \alpha < 10\%$ ) after which increases up to 260 kJ/mol.

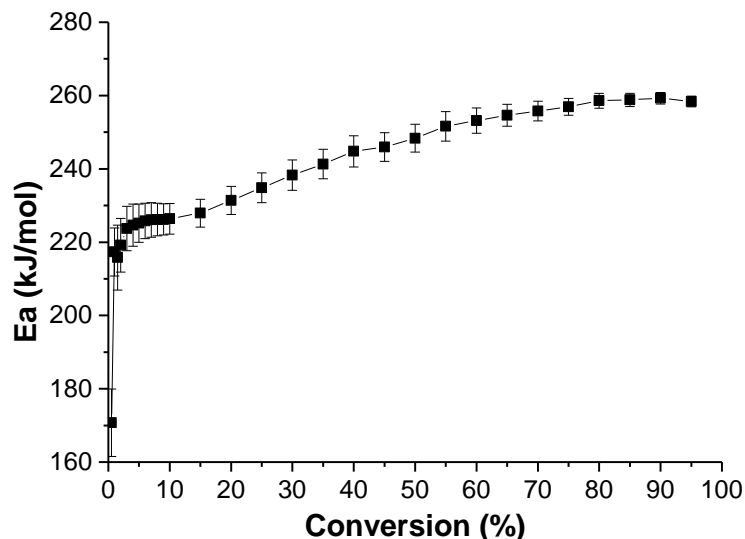


Figure 49. Plot of activation energies for HDPE degradation in N<sub>2</sub> as function of mass loss percentage.

This behavior suggests that HDPE degradation rate decreases proportionally to conversion ( $\alpha$ ), as confirmed by thermal endurance plot (figure 50), where the curves result more spaced at higher conversion values.

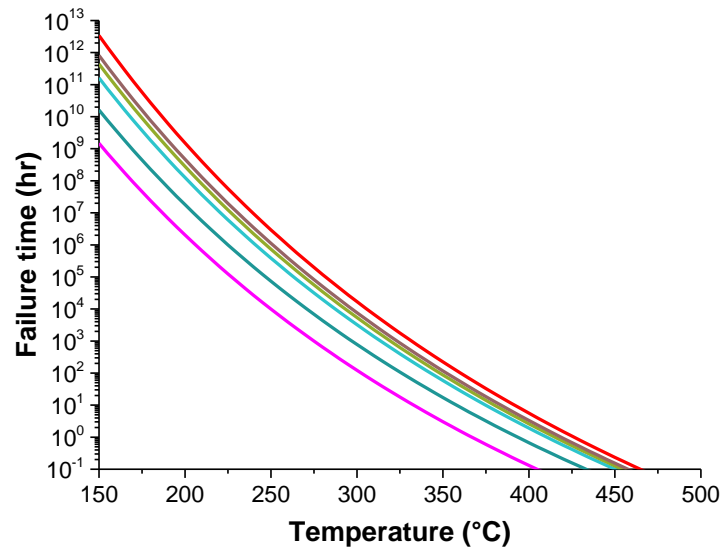


Figure 50. Thermal endurance curves of HDPE in nitrogen (left) and air environment (right) for conversion percentages of 2%, 5%, 10%, 30%, 40%, 50% and 75%, ordered from left to right

## 4.2. Applicability of Ozawa-Flynn-Wall method

For what concerns tests performed at 200°C and 220°C, no mass loss have been recorded even for 24 hours test. This characteristic have been confirmed by Capone et al. work [80], where a minimum degradation temperature of 230°C have been observed.

For tests performed at 250°C (figure 51), instead, ASTM E1641 and E1877 lead to an overestimation of thermal endurance of a magnitude inversely proportional to sample mass and area-volume ratio (i.e. A/V). The possible reasons for this behavior could be the different kinetic order for oxidation reaction ( $n \neq 1$ ) or diffusion limited oxidation (DLO).

In the first case the use of a more accurate and complex model has to be exploited, e.g. jump factor method used by Peterson et al. [79].

In the second one, PS oxidation is hindered by slow oxygen diffusion and, therefore, oxidation reactions occur mostly close to the exposure surface, while bulk polymeric chains undergo just thermal degradation. In order to overcome this issue, here is proposed an original method which is based on a vertical shift of thermal endurance curve proportional to the ratio between environment exposed area and volume. Indeed, for a constant volume, higher exposed surface lead to a better oxygen diffusion throughout bulk and, therefore, DLO process becomes less significant.

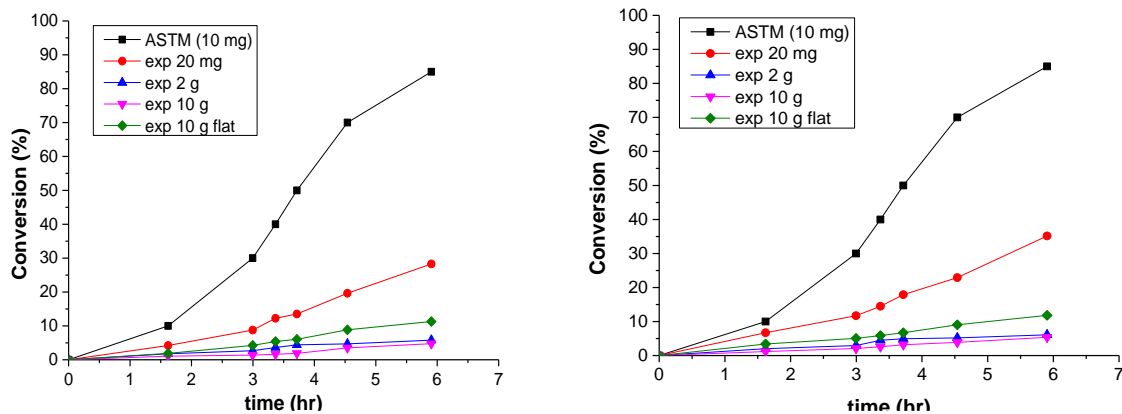


Figure 51. Degradation percentages of samples S1 (red), S2 (blue), S3 (violet) and S4 (green) for PS N2982 compared to the ones obtained by mean of OFW (black) obtained for PS N2982 (left) and PS N2380 (right)

According to this procedure, a shift factor ( $k_m$ ) is calculated by performing the ratio between the degradation times obtained experimentally ( $t_f(exp)$ ) and the one estimated by mean of OFW method ( $t_f(OFW)$ ) for the same conversion value ( $\alpha$ ) and temperature:

$$k_m = \frac{t_f(exp)}{t_f(OFW)} \quad (\text{Eq. 50})$$

Subsequently, thermal endurance curves resulting from OFW method are multiplied by  $k_m$  in order to estimate degradation times ( $t'_f$ ) that better approximate the experimental results.

$$t'_f = k_m t_f \quad (\text{Eq. 51})$$

### 4.2.1. Polystyrene N2982

The obtained values for  $T=250^\circ\text{C}$  have been compared to experimental ones and resulting plots are presented in figures 52-55. As can be seen, this method presents high accuracy for S1 sample, while, at lower area-volume ratios, presents a threshold value after which a divergent behavior with respect to real values is observed.

Moreover, this method is characterized by a slight underestimation of degradation percentages during the initial stage of the process.

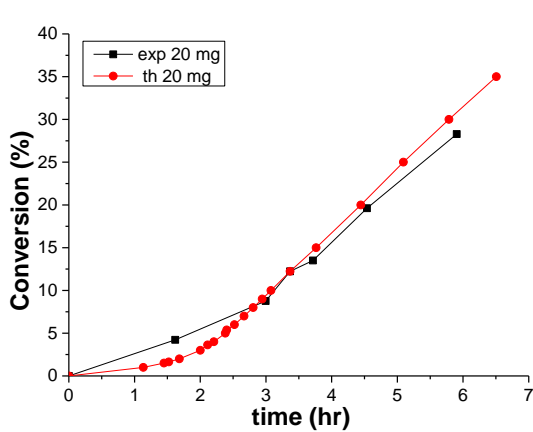


Figure 52. Degradation percentages of sample S1 obtained experimentally (black) and by mean of the proposed method

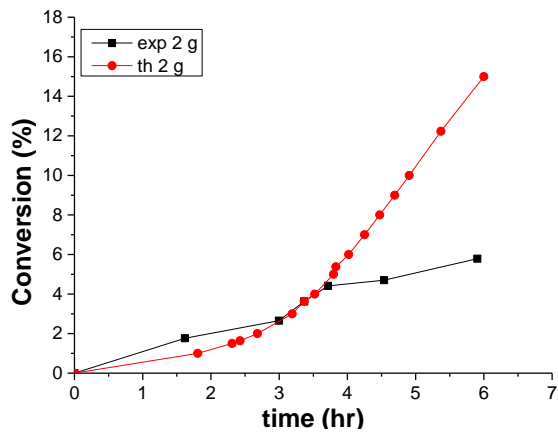


Figure 53. Degradation percentages of sample S2 obtained experimentally (black) and by mean of the proposed method

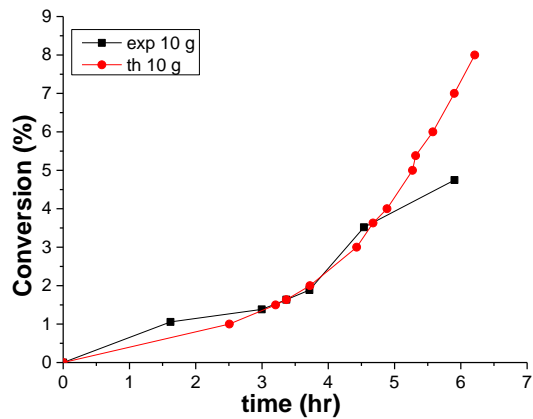


Figure 54. Degradation percentages of sample S3 obtained experimentally (black) and by mean of the proposed method

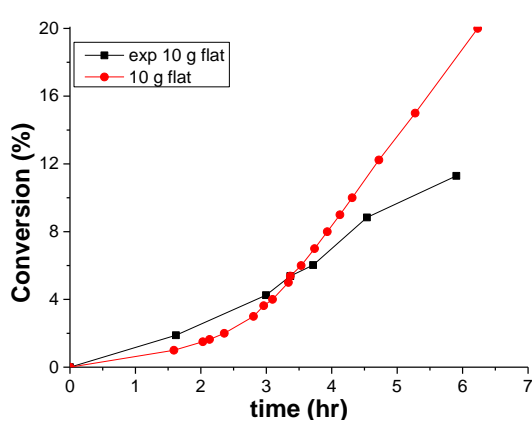


Figure 55. Degradation percentages of sample S4 obtained experimentally (black) and by mean of the proposed method

In conclusion, as can be seen in figure 56, an inverse proportionality holds between shift factor ( $k_m$ ) and are-volume ratio, which confirms the previously mentioned diffusing limited oxidation (DLO) process.

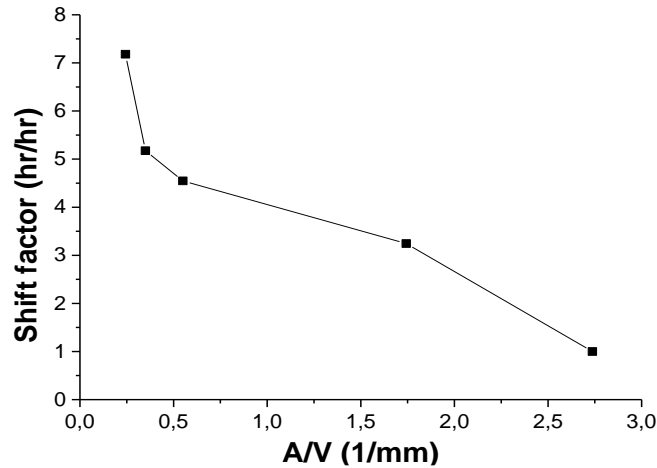


Figure 56. Relation between shift factor and area-volume ratio for PS N2982

For what concerns tests performed at 200°C and 220°C, no mass loss have been recorded even after 24 hours. This characteristic have been confirmed by Capone et al. work [80], where a minimum degradation temperature  $T=230^{\circ}\text{C}$  have been observed.

#### 4.2.2. Polystyrene N2380

The above described procedure have been applied to analogous samples made in polystyrene N2380, whose results have been plotted in figures 57-60.

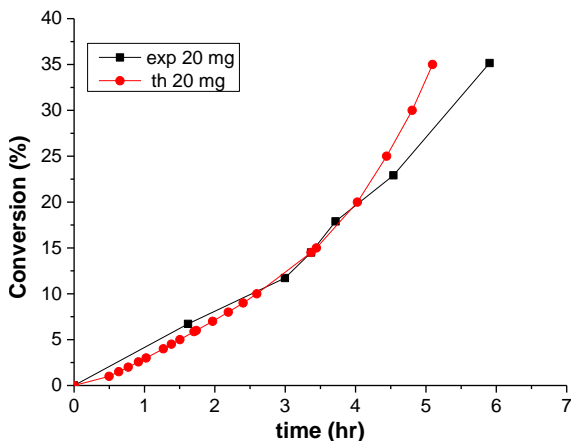


Figure 57. Degradation percentages of sample S1 obtained experimentally (black) and by mean of the proposed method

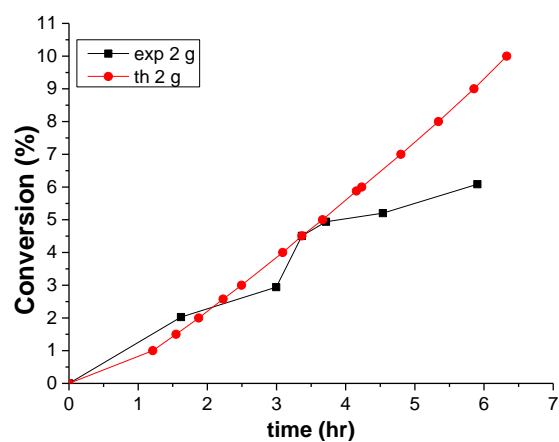


Figure 58. Degradation percentages of sample S2 obtained experimentally (black) and by mean of the proposed method

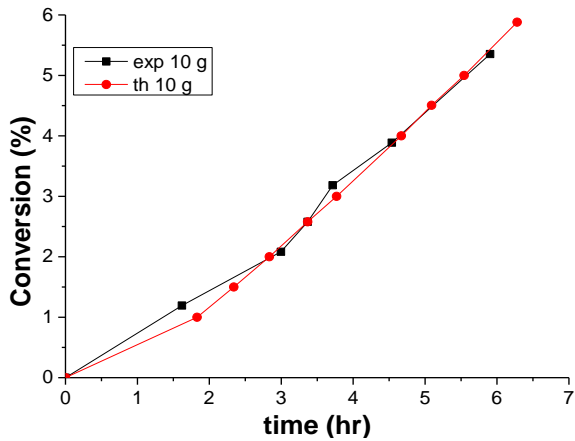


Figure 59. Degradation percentages of sample S3 obtained experimentally (black) and by mean of the proposed method

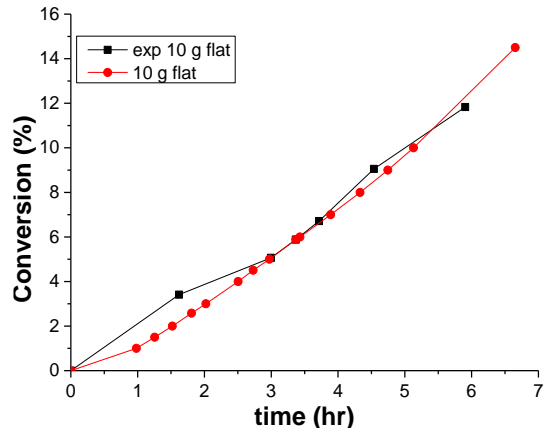


Figure 60. Degradation percentages of sample S4 obtained experimentally (black) and by mean of the proposed method

As can be noticed, calculated data present generally higher accuracy (except for sample S2) for high molecular weight polystyrene and, moreover, the estimated shift factor trend (figure 61) is characterized by a more linear dependency to area-volume ratio.

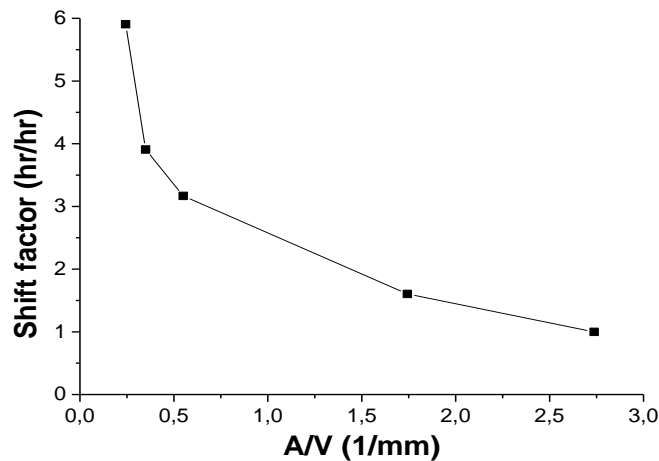


Figure 61. Relation between shift factor and area-volume ratio for PS N2380

## 5. Conclusions

Polymeric materials have widespread applications in everyday life because of their versatility, cost-effectiveness and ease of processability. However, their properties are characterized by a strong dependence on processing method and service environment, hence, a prediction of behavior of these materials is of the uttermost importance in the industrial sector.

Due to the long required time and high cost which characterize usually-employed techniques, a short-term analytical method, performed by means of various thermogravimetric analyses, was studied as an alternative way to forecast the thermal stability of polymeric materials, in accordance with ASTM standards.

An assessment of this methods was performed by estimating the thermal endurance in inert (nitrogen) and oxidative environment (air) of two different materials, namely high-density polyethylene (HDPE) and polystyrene at two different molecular weights (PS N2982 and PS 2380).

Results obtained for HDPE degradation in nitrogen showed a good agreement with respect to data found in literature, hence, confirming the applicability of the method for degradation in inert environment for reactions with a first order kinetic.

Analysis performed in inert environment on polystyrene N2982 highlighted the importance of an appropriate selection of heating program, suggesting the employment of heating rates in the range of 1-10°C/min, in order to perform an accurate estimation of activation energy and, therefore, of thermal endurance.

Results of studies performed on both polystyrenes pinpointed that molecular weight have negligible effect over degradation kinetic in nitrogen environment, while, for thermal oxidation, higher molecular weights resulted in a consistent increase of degradation resistance, especially at low temperatures.

Tests performed in ventilated oven evidenced a conspicuous difference in degradation extent, emphasized for more bulky samples, between experimental and ASTM-estimated data.

The application of an appropriate shift factor, depending on the ratio between environment exposed area and volume, led to a set of results in good agreement with the experimental ones, although, the validation of this technique requires further research.

For what concerns degradation during processing, obtained results highlighted a consistent reduction of polymer molecular weight due to mechanical milling action. The outcome was in good agreement with literature papers.



## REFERENCES

1. Sudip Ray and Ralph P. Cooney, Handbook of Environmental Degradation of Materials, Chapter 9
2. Polymer Degradation and Stability, Volume 93, Issue 3, March 2008, Pages 561-584
3. Oswald, H.J. ; Turi, E. Polym. Eng. Sci.1965, 5, 152.
4. Wyzgosky, M.G. J. Appl. Polym. Sci. 1981, 26, 1689.
5. Gillen, K.T.; Bernstein, R.; Clough, R.L.; Celina, M. Polym. Degrad. Stab. 2006, 91, 2146.
6. Bolland, J. L.; Gee, Trans. Faraday Soc. 1946, 42, 236.
7. Bolland, J. L. Trans. Faraday Soc. 1948, 44, 669.
8. Denisov, E.T. in Developments in Polymer Stabilization, Vol. 5, ed. G. Scott, Applied Science Publisher, London, 1982, pp. 23-40.
9. Niki, E.; Decker C.; Mayo, F.R. J. Polym. Sci. Polym. Chem. Ed. 1973, 11, 2813.
10. Decker, C.; Mayo, F.R. J. Polym. Sci. Polym. Chem. Ed. 1973, 11, 2847.
11. Mayo, F.R. Macromolecules 1978, 11, 942.
12. Garton, A.; Carlsson, D.J.; Wiles, D.M. Makromol. Chem. 1980, 181, 1841-1846.
13. Chien, J.C.W.; Jabloner, H.J. J. Polym. Sci. Polym. Chem. Ed. 1968, 6, 393.
14. Zolotova, N.V.; Denisov, E.T. J. Polym. Sci. Polym. Chem. Ed. 1971, 9, 3311
15. Chien, J.C.W.; Boss, C.R. J. Polym. Sci. Polym. Chem. Ed. 1967, 5, 3091
16. Russell, G.A. J. Am. Chem. Soc. 1975, 79, 387
17. H. G. Barth & F. J. Carlin Jr. (1984) A Review of Polymer Shear Degradation in Size-Exclusion Chromatography, Journal of Liquid Chromatography, 7:9, 1717-1738
18. Bird, R. B., Armstrong, 8. C. and Hassager, O., Dynamics of Polymeric Liquids, Vol. 1, John Wiley h Sons, N.Y., 1977, p. 61.
19. Casale, A., Porter, R. S. and Johnson J. F., The Uechanochemistry of High Polymers, Rubber Chem. and Technol., 44\_, 534 (1971)
20. Frenkel, Y. I., Orientation and Rupture of Linear Macromolecules in Dilute Solution under the Influence of Viscous Flow, Acta Physiochim. USSR, 19. 51 ,1944
21. C. Capone, L. Di Landro, F. Inzoli, M. Penco, L. Sartore, Thermal and Mechanical Degradation During Polymer Extrusion Processing, Polymer engineering and science 2007
22. K. Arisawa and R.S. Porter, J. Appl. Polym. Sci., 14, 879 (1970).
23. K.P. Goetze and R.S. Porter, J. Appl. Polym. Sci., 35, 189 (1971).
24. E. Yousif, R. Haddad, photodegradation and photostabilization of polymers, especially polystyrene: review, SpringerPlus 2013, 2:398
25. V.S. Ramachandran, R.M. Paroli, J.J. Beaudoin, A.H. Delgado, Handbook of thermal analysis of construction materials. No Wich, New York, Noyes Publications, William Andrew Publishing, 2002, pp. 1-5, 9-30
26. T. Ozawa, "Thermal analysis - review and prospect", Thermochemica Acta 355 (2000) 35-42
27. A. W. COATS AND J. P. REDFERN, "Thermogravimetric Analysis",
28. Keattch, C. J., and Redfern, J. P., J. Less Common Metals, 1962, 4, 460
29. Guiochon, G., Anal. Chem., 1961, 33, 1124

30. Newkirk, A. E., *Ibid.*, 1960, 32, 1558.
31. Pellon, J. ., paper presented at the International Symposium on Inorganic Polymers, Nottingham , 1961
32. Richer, A., *Inst. Rech. de la Sidei.ugie*, 1960, Series A, No. 187.
33. Cueilleron, J., and Hartmanshenn, O., *Bull. SOC. Chim. France*, 1959, 172.
34. Mauras, H., *Ibid.*, 1960, 260
35. Berlin, A., and Robinson, R. J., *Anal. Chim. Acta*, 1962, 27, 50
36. Paulik, F., Erdey, L., and Gal, S., *Bergakadrmie*, 1962, 14, 21.
37. Moore, W. R., and Donnelly, E., paper given at the Conference on Advances in Polymer Science and Technology, London, May, 1963
38. Gilbert, J. B., Kipling, J. J., McEnaney, B., and Sherwood, J. N., *Polymer*, 1962, 3, 1
39. J.D. Sewry, M.E. Brown, *Thermochim. Acta* 390 (2002) 217.
40. A.K. Galwey, M.E. Brown, in: M.E. Brown (Ed.), *Handbook of Thermal Analysis and Calorimetry*, vol. 1, Elsevier, Amsterdam, 1998, p. 147.
41. L. Abdelouahed, S. Leveneur, L. Vernieres-Hassimi, L. Balland, B. Taouk, "Comparative investigation for the determination of kinetic parameters for biomass pyrolysis by thermogravimetric analysis", *J Therm Anal Calorim* (2017) 129:1201–1213
42. Soria-Verdugo A, Garcí ´a-Hernando N, Garcia-Gutierrez LM, Ruiz-Rivas U. Analysis of biomass and sewage sludge devolatilization using the distributed activation energy model. *Energy Convers Manag*. 2013; 65:239–44.
43. M. Venkatesh, P. Ravi and Surya P. Tewari, "Isoconversional Kinetic Analysis of Decomposition of Nitroimidazoles: Friedman method vs Flynn–Wall–Ozawa Method", *J. Phys. Chem. A* 2013, 117, 10162–10169
44. A. Brems, J. Baeyens, J. Beerlandt, and R. Dewil, "Thermogravimetric pyrolysis of waste polyethylene-terephthalate and polystyrene: A critical assessment of kinetics modelling," *Resour. Conserv. Recycl.*, vol. 55, no. 8, pp. 772–781, Jun. 2011.
45. E. Baroni, K. Tannous, Y. J. Rueda-Ordonez, L. K. Tinoco-Navarro, "The applicability of isoconversional models in estimating the kinetic parameters of biomass pyrolysis", *J Therm Anal Calorim* (2016) 123:909–917
46. D. R. Dowdy, "MEANINGFUL ACTIVATION ENERGIES FOR COMPLEX SYSTEMS" *Journal of Thermal Analysis*", Vol. 32 (1987) 137-147
47. M. C. Celina, "Review of polymer oxidation and its relationship with materials performance and lifetime prediction," *Polym. Degrad. Stab.*, vol. 98, no. 12, pp. 2419–2429, Dec. 2013.
48. K. Slopiecka, P. Bartocci, F. Fantozzi, "Thermogravimetric analysis and Kinetic study of poplar wood pyrolysis" *Third International Conference on Applied Energy - 16-18 May 2011* pag. 1687-1698
49. N. Kongkaewa , W. Pruksakitb, S. Patumsawada, "Thermogravimetric Kinetic Analysis of the Pyrolysis of Rice Straw", *Energy Procedia* 79 ( 2015 ) 663 – 670
50. J. Yang, & C. Roy, Using DTA to quantitatively determine enthalpy change over a wide temperature range by the "mass difference baseline method". *Thermochimica*, 333, 131–140, 1999.
51. H. Chan Sze, "An overview of thermal analysis of polymers", *Asean Journal on Science and technology for development*, 3(1)(1986) 36-54

52. A. Zambrano, G.Castellar, W.Vallejo, I.Piñeres, M.M. Cely, J.Valencia, Aproximación conceptual al análisis térmico y sus principales aplicaciones, "Conceptual approach to thermal analysis and its main applications". *Prospectiva*, Vol 15, N° 2, 117-125, 2017.
53. S.L. Boersma, *J. Am. Ceram. Soc.* 38 (1955) 281
54. P.J. Haines, Introduction to thermal methods, in *Thermal methods of analysis. Principles, applications and problems* Netherlands, 1995. pp. 279-289.
55. W. Zielenkiewicz, "Towards classification of calorimeters". *Journal of Thermal Analysis and Calorimetry*, 91, 663-71, 2008.
56. A. Guyot, Recent Developments in the Thermal Degradation of Polystyrene-A Review, *Polymer Degradation and Stability* 15 (1986) 219-235
57. G. G. Cameron and I. T. McWalter, *Europ. Polym. J.*, 17, 253 (1981)
58. L. A. Wall, S. Strauss, R. E. Florin and L. J. Fetters, *J. Research Nat. Bureau of Standards*, 77, 157 (1973)
59. H. H. G. Jellinek, Thermal degradation of polystyrene, Part II, *J. Polymer Sci.* <10, 1 (1949)
60. Jinbao Huang, Chao Heb, Xinsheng Lic, Guiying Pana, Hong Tonga, Theoretical studies on thermal degradation reaction mechanism of model compound of bisphenol A polycarbonate
61. Flynn, J.H., and Wall, L.A., "A Quick, Direct Method for the Determination of Activation Energy from Thermogravimetric Data," *Polymer Letters*, Vol 4, 1966, pp. 323–328.
62. Ozawa, T., "A New Method of Analyzing Thermogravimetric Data," *Bulletin of the Chemical Society of Japan*, Vol 88, 1965, pp. 1881–1886.
63. Doyle, C. D. (1961), "Kinetic analysis of thermogravimetric data". *J. Appl. Polym. Sci.*, 5: 285-292.
64. J. J. Xu and C. A. Kaminski, "Temperature index of electrical insulations by mTGA," *J. Test. Eval.*, vol. 42, no. 6, 2014
65. Krizanovsky, L., and Mentlik, V., "The Use of Thermal Analysis to Predict the Thermal Life of Organic Electrical Insulating Materials," *Journal of Thermal Analysis*, Vol 13, 1978, pp. 571–580. 33.
66. Skoog, D.A., West, D. M., Holler, F. J., Crouch, S. R., *Fundamentals of Analytical Chemistry*, Thompson Brooks/Cole, 8th ed, 2004, pp. 127–133.
67. T. BREMNER and A. RUDIN, Melt Flow Index Values and Molecular Weight Distributions of Commercial Thermoplastics, *Journal of Applied Polymer Science* · January 1990
68. International Organization for Standards, "ISO 1133 - Determination of the melt mass flow rate (MFR) and melt volume flow rate (MVR) of thermoplastics," vol. 2011, 2011.
69. American Society for Testing and Materials, "ASTM D 1238-04 - Standard Test Method for Melt Flow Rates of Thermoplastics by Extrusion Plastometer"
70. M. R. AMBLER, " Molecular Weight Characterization of Polybutadiene Rubber with High Molecular Weight and Broad Molecular Weight Distribution", *Journal of Applied Polymer Science*, Vol. 25,901-920 (1980)
71. American Society for Testing and Materials "Standard Practice for Dilute Solution Viscosity of Polymers", 2016
72. International Organization for Standards, " ISO 1628 – Plastics- Determination of the viscosity of polymers in dilute solution using capillary viscometers", 1998

73. International Organization for Standards, "ISO 3105- Methods of test for petroleum and its products", 1994
74. American Society for Testing Materials, "ASTM D2538- Fusion of Poly(Vinyl Chloride) (PVC) Compounds Using a Torque Rheometer"
75. Underwriters Laboratories, "UL 746B: Polymeric Materials - Long Term Property Evaluations," Fourth Edi., Underwriters Laboratories, 2013.
76. K. M. Wagner, "A Study Of The Thermal Oxidative Degradation Of Polyamide 6,6 – Prediction Of The Thermal Index By A Short Term Analytical Method Versus Long Term Thermal Aging," Master's Thesis, Washington State University, 2016.
77. Flory, P. J., J Am. Chem. Soc., 1937, 59, 241
78. Aguado, J., D. P. Serrano, J. M. Escola, Ind. Eng. Chem. Res. 2008, 47, 7982–7992
79. D'Amato, Michael J., "Thermal Degradation Of High Molecular Weight Polyethylene To Obtain Low Molecular Weight Polyethylene Wax" (2012). Theses and dissertations. Paper 1310.
80. Oakes, W.G., R.B. Richards, J. Chem.Soc. 2929-2935(1949)
81. Gao, Z., I. Amasaki, M. Nakada, J. Anal. Appl. Pyrolysis 67 (2003) 1–9
82. J. D. Peterson, S. Vyazovkin, C. A. Wight, Macromol. Chem. Phys., 202 (2001) No. 6
83. Westerhout, R.W.J., J. Waanders, J. A. M. Kuipers, W. P. M. van Swaaij, Ind. Eng. Chem. Res. 1997, 36, 1955-196
84. Brabender datasheet, available at: <https://www.brabender.com/en/chemical/products/measuring-mixer/>
85. J. H. Flynn and L. A. Wall, "General Treatment of the Thermogravimetry of Polymers" JOURNAL OF RESEARCH of the National Bureau of Standards - A. Physics and Chemistry Vol. 70A, No. 6, November- December 1966
86. Arfin, Tanvir & Mohammad, F. & Yusof, Nor. (2014). Applications of polystyrene and its role as a base in industrial chemistry.
87. M.W. Collis, M.R. Mackley, "The melt processing of monodisperse and polydisperse polystyrene melts within a slit entry and exit flow", Journal of Non-Newtonian Fluid Mechanics, Volume 128, Issue 1, 2005, Pages 29-41
88. American Society for Testing Materials, "ASTM E2550-17 - Standard Test Method for Thermal Stability by Thermogravimetry"
89. American Society for Testing Materials, "ASTM E1641-16 -Standard Test Method for Decomposition Kinetics by Thermogravimetry Using the Ozawa/Flynn/Wall Method"
90. American Society for Testing Materials, "ASTM E1877-17 - Standard Practice for Calculating Thermal Endurance of Materials from Thermogravimetric Decomposition Data"
91. International Organization for Standards, "BS EN ISO 11358 — Thermogravimetry (TG) of polymers", 2014
92. Yuan, Y., Johnson, F. and Cabasso, I. (2009), Polybenzimidazole (PBI) molecular weight and Mark-Houwink equation. J. Appl. Polym. Sci., 112: 3436-3441
93. Alonso A., Lázaro M., Lázaro P., Lázaro D., Alvear D., "LLDPE kinetic properties estimation combining thermogravimetry and differential scanning calorimetry as optimization targets"(2019) Journal of Thermal Analysis and Calorimetry, 138 (4), pp. 2703-2713

94. Versalis datasheet available at: "<https://www.granulat.com.pl/media/pdf/edistir%20n%202982.pdf>"
95. Versalis datasheet available at: "[https://www.versalis.eni.com/irj/go/km/docs/versalis/Contenuti%20Versalis/EN/Documenti/Prodotti/Stirenici/Schede%20Tecniche/GPPS%20HIPS/Edistir%20N%202380%20\(ENG\).pdf](https://www.versalis.eni.com/irj/go/km/docs/versalis/Contenuti%20Versalis/EN/Documenti/Prodotti/Stirenici/Schede%20Tecniche/GPPS%20HIPS/Edistir%20N%202380%20(ENG).pdf)"
96. Mehrdad Seifali Abbas-Abadi, Mehdi Nekoomanesh Haghghi, Hamid Yeganeh
97. A.S. Abu-Bakar, K.A.M. Moinuddin Effects of Variation in Heating Rate, Sample Mass and Nitrogen Flow on Chemical Kinetics for Pyrolysis, available at: "<https://people.eng.unimelb.edu.au/imarusic/proceedings/18/282%20-%20Abu%20Bakar.pdf>"